RIEMANN INVARIANT MANIFOLDS FOR THE MULTIDIMENSIONAL EULER EQUATIONS[*]

TASSO LAPPAS[†], ANTHONY LEONARD[†], AND PAUL E. DIMOTAKIS[†]

Abstract. A new approach for studying wave propagation phenomena in an inviscid gas is presented. This approach can be viewed as the extension of the method of characteristics to the general case of unsteady multidimensional flow. A family of spacetime manifolds is found on which an equivalent one-dimensional (1-D) problem holds. Their geometry depends on the spatial gradients of the flow, and they provide, locally, a convenient system of coordinate surfaces for spacetime. In the case of zero-entropy gradients, functions analogous to the Riemann invariants of 1-D gas dynamics can be introduced. These generalized Riemann invariants are constant on these manifolds and, thus, the manifolds are dubbed Riemann invariant manifolds (RIM). Explicit expressions for the local differential geometry of these manifolds can be found directly from the equations of motion. They can be space-like or time-like, depending on the flow gradients. This theory is used to develop a second-order unsplit monotonic upstream-centered scheme for conservation laws (MUSCL)-type scheme for the compressible Euler equations. The appropriate RIM are traced back in time, locally, in each cell. This procedure provides the states that are connected with equivalent 1-D problems. Furthermore, by assuming a linear variation of all quantities in each computational cell, it is possible to derive explicit formulas for the states used in the 1-D characteristic problem.

1. Introduction. A great deal of work has contributed to the understanding of nonlinear hyperbolic systems of equations, such as the compressible Euler equations. The main ingredients in the study of such systems are the concept of characteristic surfaces and the theory describing their properties. See, for example, Courant and Hilbert (1963).

Characteristic surfaces in spacetime can be viewed as propagating wave fronts and are usually interpreted as disturbance waves in the system that the equations represent. This picture becomes more useful and much clearer in the special case of systems in two independent variables, where one of the independent variables is time. It is in this special case that most of the work has been done. It is useful to think about unsteady 1-D gas dynamics as an example of this case. The characteristic surfaces now become curves in two-dimensional (2-D) spacetime. This is a serious simplification, since now there are only two possible propagation directions for waves, the positive and negative spatial directions. Moreover, the equations written along these characteristic directions are greatly simplified. Under certain conditions, one can define functions that are invariant along these paths. They are the familiar Riemann invariants. The solution can be written, locally, in spacetime as a superposition of these characteristic waves. Each invariant satisfies a simple convective equation; thus, the original system of equations is replaced by an equivalent set of convective scalar equations. This is the decomposition into the characteristic scalar fields. For gas

dynamics one has convective waves that propagate with the local fluid velocity and the acoustic waves that propagate with the local speed of sound, in the reference frame of the fluid.

When there are more than two independent variables, such as in the case of unsteady multidimensional flow in a gas, the situation becomes more difficult. The characteristic curves now become characteristic manifolds in a higher dimensional spacetime. These manifolds can be viewed as being generated, locally, by appropriate vector fields. The directions of these vector fields are dubbed *bicharacteristic* directions and the vector fields are generators of a cone which is called the *bicharacteristic cone.* This cone is tangent to the characteristic manifolds. Now, there are more than just two available directions for the propagation of waves. This difficulty is to be expected, but in addition to this, the equations no longer simplify the same way as in 1-D flow. The equations can be written along the bicharacteristic directions and the characteristic decomposition of the original system into scalar fields can be carried out, formally, as in the case of two independent variables. But now, the equations are not simpler in any way than the original system. Riemann invariants no longer exist along these paths and the solution cannot be written as a simple superposition of waves as before.

In the present paper a different type of local wave decomposition, the RIM decomposition, is given for the compressible Euler equations, which holds under slightly different smoothness assumptions than those for the familiar characteristic decomposition. Manifolds in spacetime are found along which the 1-D characteristic equations hold. One can integrate them numerically by using techniques that work with 1-D problems. In the absence of entropy gradients, integration of these equations results in the familiar Riemann invariants. If N is the number of spatial dimensions, there is, in general, an $(N-1)$-parameter family of such N-dimensional manifolds in spacetime on which the Riemann invariants are constant. Explicit expressions for the direction and speed of propagation of the wave fronts that these manifolds represent are found directly from the Euler equations. It turns out that they depend on particular combinations of the spatial pressure and velocity gradients.

The ability to write explicit expressions for these waves is what makes this decomposition very useful from theoretical and computational points of view. Knowledge of the spatial gradients in the flow contains a great deal more information, locally, than that given by the familiar characteristic decomposition. Moreover, the combinations of spatial gradients that are important are revealed in a very natural way by seeking paths along which the 1-D equations hold. It is these combinations that pick out important directions of local wave propagation. Moreover, it becomes apparent that it is possible in some cases to compute the solution at a certain point in spacetime using information from outside its domain of dependence. This is because the appropriate Riemann invariant waves may be traveling at speeds greater than the largest characteristic speed. Also, it is possible for a subsonic flow to exhibit, locally, a "hyperbolic"-type behavior depending on the flow gradients. This result is interesting and its relation to the theorems of uniqueness is discussed. Details on the proofs of these uniqueness theorems can be found in Courant and Hilbert (1963), Friedrichs and Lax (1965), and Kato (1975).

The proposed RIM wave decomposition is also useful in the context of the recent high-resolution schemes developed for computing hyperbolic systems of equations such as the compressible Euler equations. These high-resolution schemes, such as the ENO and TVD schemes, described by Harten et al. (1987) and Harten (1983, 1984), the

λ-scheme introduced by Moretti (1979), the MUSCL scheme by van Leer (1979), PPM by Colella and Woodward (1984), and Roe's approximate Riemann solver given by Roe (1981), take advantage of the extensive theory on hyperbolic systems of equations in two independent variables. The main idea is to develop stable and at least second-order accurate schemes for computing a scalar convective equation. Systems of equations are then treated by using the characteristic decomposition into scalar fields, which works very well for systems in just two independent variables. Weak solutions, i.e., discontinuous solutions, are allowed by using a conservative formulation and making sure that the discretization of the scalar field equations is at least second-order accurate, but does not generate spurious oscillations. In the context of gas dynamics the above procedure can be viewed as using, locally at each computational cell interface, the method of characteristics to compute the appropriate flux terms. Since discontinuous solutions are expected, the method is generalized by solving an appropriate Riemann problem. The solution to this Riemann problem has to reduce to a second-order solution to the characteristic scalar field equations in the absence of discontinuities. This is the spirit of extending to second-order accuracy the original Godunov scheme (1959).

Although the application of this idea is straightforward for the 1-D case, the extension to multidimensional flows is not. Practically, these schemes are extended to more dimensions by treating the additional spatial dimensions separately. The computation is not truly multidimensional, but rather a number of separate, 1-D computations in each spatial direction. Even schemes that appear to be multidimensional (unsplit) actually use the local directions of the grid to set up and solve a 1-D Riemann problem, thus taking advantage of the 1-D results. Efforts to create a genuinely multidimensional scheme are those by Roe (1986), Hirsch and Lacor (1989), and Deconinck, Hirsch, and Peuteman (1986). A true extension of the Godunov scheme to the multidimensional case would be finding a solution to the multidimensional Riemann problem. For 1-D gas dynamics, it can be shown that the Riemann problem has a unique solution and that the general, initial value problem has a unique weak solution; see Glimm (1965) and Smoller (1983). This has not yet been done in higher dimensions.

Despite this, the RIM wave decomposition can be used to construct unsplit multidimensional schemes by finding states that are connected with equivalent 1-D problems. In what follows, the theory of RIM will be used to construct a conservative, shock-capturing scheme for unsteady, 2-D flow. The basis for the scheme is a second-order Godunov scheme (MUSCL scheme; see van Leer (1979)), which is modified to take into account the multidimensional character of the flow. The numerical fluxes are computed by tracing the appropriate RIM back in time, in order to find the states which are related with an equivalent 1-D problem. This results in a multidimensional scheme without flux splitting, i.e., a truly unsplit scheme. The application of the theory is demonstrated for 2-D flow, but the extension to three-dimensional (3-D) flow is straightforward.

2. The compressible Euler equations.

2.1. Characteristic theory. The equations of interest are those governing the 3-D inviscid flow of a compressible fluid. All the results presented hold for the general 3-D case, although for visualization purposes the figures are given for 2-D flow. It is much easier to visualize a 3-D spacetime than a four-dimensional (4-D) one. The equations of motion can be written in the nonconservative form

$$\frac{\partial \rho}{\partial t} + \nabla \cdot (\rho \mathbf{u}) = 0 \,,$$

(1)
$$\frac{\partial \mathbf{u}}{\partial t} + \mathbf{u} \cdot \nabla \mathbf{u} + \frac{1}{\rho} \nabla p = 0 \,,$$

$$\frac{\partial p}{\partial t} + \mathbf{u} \cdot \nabla p + \rho a^2 \nabla \cdot \mathbf{u} = 0 \,,$$

where ρ is the density, p is the pressure, $\mathbf{u} = (u, v, w)^{\mathrm{T}}$ is the velocity vector, and a is the speed of sound. Eqs. (1) can be written in the general form

(2)
$$\frac{\partial U}{\partial t} + A_x \frac{\partial U}{\partial x} + A_y \frac{\partial U}{\partial y} + A_z \frac{\partial U}{\partial z} = 0 \,,$$

where

$$U = \begin{pmatrix} \rho \\ u \\ v \\ w \\ p \end{pmatrix}, \qquad A_x = \begin{pmatrix} u & \rho & 0 & 0 & 0 \\ 0 & u & 0 & 0 & 1/\rho \\ 0 & 0 & u & 0 & 0 \\ 0 & 0 & 0 & u & 0 \\ 0 & \rho a^2 & 0 & 0 & u \end{pmatrix},$$

(3)
$$A_y = \begin{pmatrix} v & 0 & \rho & 0 & 0 \\ 0 & v & 0 & 0 & 0 \\ 0 & 0 & v & 0 & 1/\rho \\ 0 & 0 & 0 & v & 0 \\ 0 & 0 & \rho a^2 & 0 & v \end{pmatrix}, \qquad A_z = \begin{pmatrix} w & 0 & 0 & \rho & 0 \\ 0 & w & 0 & 0 & 0 \\ 0 & 0 & w & 0 & 0 \\ 0 & 0 & 0 & w & 1/\rho \\ 0 & 0 & 0 & \rho a^2 & w \end{pmatrix}.$$

There are five unknown functions defined on 4-D spacetime, i.e., $N = 3$ spatial dimensions. One can easily specialize the following results to the case $N = 2$ or $N = 1$. This is a hyperbolic system and its characteristic manifolds can be found in a straightforward way. There is a convective characteristic surface which is locally generated by the fluid velocity $\mathbf{u}$ and a family of acoustic characteristic surfaces that are generated by the local bicharacteristic vectors $\mathbf{u} + a\mathbf{n}$, where $\mathbf{n}$ is a spatial unit vector.

The differential equations that hold on the characteristic manifolds can be found, formally, by attempting to diagonalize the matrices that appear in (2). Given an arbitrary unit vector $\mathbf{n}$, a straightforward calculation yields the left and right eigenvectors of the matrix $\mathbf{n} \cdot \mathbf{A}$, where $\mathbf{A} = (A_x, A_y, A_z)^{\mathrm{T}}$. The differential equation that holds along a characteristic ray can be found by multiplying from the left by the appropriate eigenvector; i.e,

(4)
$$\left\langle l_k, \frac{\partial U}{\partial t} \right\rangle + \left\langle l_k, A_m \frac{\partial U}{\partial x_m} \right\rangle = 0 \,, \qquad k = 1, \ldots, M \,,$$

where $\langle \cdot, \cdot \rangle$ is the usual inner product in $\Re^M$ and M is the number of equations, i.e., $M = 5$. The summation convention is adopted for all repeated indices. By multiplying from the left with the left eigenvectors l_k corresponding to the acoustic manifold of the Euler equations, one finds the differential equation, which holds along the bicharacteristic, $\dot{\mathbf{x}}(t) = \mathbf{u} + a\mathbf{n}$,

(5)
$$\left[\frac{\partial p}{\partial t} + (\mathbf{u} + a\mathbf{n}) \cdot \nabla p \right] + \rho a \mathbf{n} \cdot \left[\frac{\partial \mathbf{u}}{\partial t} + (\mathbf{u} + a\mathbf{n}) \cdot \nabla \mathbf{u} \right]$$
$$+ \rho a^2 \left[\nabla \cdot \mathbf{u} - \mathbf{n} \cdot (\nabla \mathbf{u}) \mathbf{n} \right] = 0 \,.$$

Using index notation and dividing through by ρa,

$$
(6) \qquad
\begin{aligned}
\frac{1}{\rho a}\left[\frac{\partial p}{\partial t} + (u_j + a n_j)\frac{\partial p}{\partial x_j}\right] + n_i \left[\frac{\partial u_i}{\partial t} + (u_j + a n_j)\frac{\partial u_i}{\partial x_j}\right] \\
+ a\left(\delta_{ij} - n_i n_j\right)\left(\frac{\partial u_i}{\partial x_j}\right) = 0 ,
\end{aligned}
$$

where δ_{ij} is the Kronecker delta. Since the tensor $\delta_{ij} - n_i n_j$ is symmetric,

$$
(7) \qquad G_n \equiv \left(\delta_{ij} - n_i n_j\right)\left(\frac{\partial u_i}{\partial x_j}\right) = \left(\delta_{ij} - n_i n_j\right) S_{ij} ,
$$

where

$$
S_{ij} \equiv \frac{1}{2}\left(\frac{\partial u_i}{\partial x_j} + \frac{\partial u_j}{\partial x_i}\right)
$$

is the rate of strain tensor. Only the symmetric part of the velocity-gradient tensor enters in the term G_n.

The significance of (5) can be seen by deriving it in a way that is not related to the concept of characteristic manifolds. Consider an arbitrary, spatial, unit vector $\mathbf{n}$. The last two equations in (1) can be combined to give (5). The momentum equation can be written as follows, by taking its inner product with the vector $\rho a \mathbf{n}$ and adding and subtracting the term $\rho a^2 \mathbf{n}\cdot(\nabla\mathbf{u})\,\mathbf{n}$; i.e.,

$$
\frac{\partial \mathbf{u}}{\partial t} + \mathbf{u}\cdot\nabla\mathbf{u} + \frac{1}{\rho}\nabla p = 0
$$

$$
\Rightarrow \qquad \rho a \mathbf{n}\cdot\left[\frac{\partial \mathbf{u}}{\partial t} + (\mathbf{u} + a\mathbf{n})\cdot\nabla\mathbf{u}\right] - \rho a^2 \mathbf{n}\cdot(\nabla\mathbf{u})\,\mathbf{n} + a\mathbf{n}\cdot\nabla p = 0 .
$$

The energy equation can be written

$$
\frac{\partial p}{\partial t} + \mathbf{u}\cdot\nabla p + \rho a^2 \nabla\cdot\mathbf{u} = 0
$$

$$
\Rightarrow \qquad \frac{\partial p}{\partial t} + (\mathbf{u} + a\mathbf{n})\cdot\nabla p + \rho a^2 \nabla\cdot\mathbf{u} - a\mathbf{n}\cdot\nabla p = 0 .
$$

Adding the two equations gives (5).

It is clear from this derivation that this equation holds for an arbitrary vector $\mathbf{n}$. It gives the relation between velocity changes and pressure changes along the direction $\dot{\mathbf{x}} = \mathbf{u} + a\mathbf{n}$. It is our knowledge of the characteristic surfaces which allows us to identify these directions as the generating rays of the acoustic characteristic manifold, i.e., the bicharacteristics. It is also important to notice that it is really a family of equations. By fixing $\mathbf{n}$ to be a unit vector, it is easy to see that (5) or (6) is actually an $(N-1)$-parameter family of equations. Indeed, for 2-D flow $(N = 2)$, the vector $\mathbf{n}$ is constrained to the unit circle and for 3-D flow it is constrained to the surface of the unit sphere. This is important because, although they are all dependent equations and consistent with the original system (1), a particular choice of $\mathbf{n}$ may be optimal for computational purposes.

If there are no entropy gradients, then (5) can be further simplified. Define the thermodynamic state variable W by

$$(8) \qquad W \equiv \int_{ds=0} \frac{dp}{\rho a} \,,$$

where the integral is performed in thermodynamic state space along a path of constant entropy s. For a perfect gas this function is simply

$$(9) \qquad W = \frac{2a}{\gamma - 1} \,,$$

where γ is the specific heat ratio. Then, (5) can be written

$$(10) \qquad \left[\frac{\partial W}{\partial t} + (\mathbf{u} + a\mathbf{n}) \cdot \nabla W \right] + \left[\frac{\partial(\mathbf{u} \cdot \mathbf{n})}{\partial t} + (\mathbf{u} + a\mathbf{n}) \nabla(\mathbf{u} \cdot \mathbf{n}) \right]$$
$$+ a \left[\nabla \cdot \mathbf{u} - \mathbf{n} \cdot (\nabla \mathbf{u}) \, \mathbf{n} \right] = 0 \,.$$

The vector $\mathbf{n}$ is assumed to be arbitrary but fixed. One can define a family of functions given by

$$(11) \qquad R_n \equiv W + \mathbf{u} \cdot \mathbf{n} \,.$$

These functions are going to be the generalization of the familiar Riemann invariants of 1-D flow. Equation (10) can now be written

$$(12a) \qquad \frac{\partial R_n}{\partial t} + (\mathbf{u} + a\mathbf{n}) \cdot \nabla R_n + a \left[\nabla \cdot \mathbf{u} - \mathbf{n} \cdot (\nabla \mathbf{u}) \, \mathbf{n} \right] = 0 \,,$$

or

$$(12b) \qquad \frac{\partial R_n}{\partial t} + (\mathbf{u} + a\mathbf{n}) \cdot \nabla R_n + aG_n = 0 \,.$$

The presence of the term $aG_n = a \left(\delta_{ij} - n_i n_j \right) S_{ij}$ in (12) acts as a source term and complicates matters in multidimensional flows. If a unit vector $\mathbf{n}$ exists, such that $G_n = 0$, then along the direction $\dot{\mathbf{x}} = \mathbf{u} + a\mathbf{n}$, (12) is integrable and $R_n = \text{const}$. By examining the form of G_n, one can see that it is not always possible to find such a direction $\mathbf{n}$. G_n is the 2-D divergence of the velocity field in the plane normal to the vector $\mathbf{n}$. For the case of 2-D flow, i.e., $N = 2$, it can be shown that a direction $\mathbf{n}$, such that $G_n = 0$, can be found only when the eigenvalues of the rate of strain tensor S are such that

$$(13) \qquad \lambda_{\min} \lambda_{\max} \leq 0 \,.$$

This condition is not always satisfied in an arbitrary flow.

One can find the equations that hold along the convective characteristic manifolds in a similar way. After this is done, it can be seen that the original Euler equations are equivalent to the following characteristic system of equations:

$$(14) \qquad \frac{\partial R_n}{\partial t} + (\mathbf{u} + a\mathbf{n}) \cdot \nabla R_n = -aG_n \,,$$
$$\frac{\partial R_0}{\partial t} + \mathbf{u} \cdot \nabla R_0 = 0 \,,$$

where

$$G_n = [\nabla{\cdot}\mathbf{u} - \mathbf{n}{\cdot}(\nabla\mathbf{u})\,\mathbf{n}] = (\delta_{ij} - n_i n_j)\,S_{ij}\ .$$

The invariant R_0 along the convective manifold can be viewed as the entropy of the system, which is constant along a streamline in the absence of shocks. Eqs. (14) constitute the characteristic decomposition of the Euler equations into scalar fields.

Consider now the special case of 1-D flow $(N = 1)$ in the x-direction. The characteristic surfaces are now characteristic curves in 2-D spacetime (t, x), and the above equations reduce to

$$(15) \qquad \frac{1}{\rho a}\frac{dp}{dt} \pm \frac{du}{dt} = 0\ ,$$

which hold along

$$(16) \qquad C_\pm\ :\ \frac{dx}{dt} = u \pm a\ .$$

In the special case of zero-entropy gradients this integrates to

$$(17) \qquad \frac{d}{dt}\,(W \pm u) = 0 \quad \Rightarrow R_\pm \equiv W \pm u = \ \text{const}\ .$$

Looking at the general multidimensional decomposition (14), there is no apparent advantage in integrating the equations of motion along the bicharacteristic directions, which can be viewed as the multidimensional extensions of the characteristics in 1-D. First, one has a multitude of bicharacteristic directions to choose from and second, the equations of motion do not greatly simplify because of the presence of the source-like term G_n. The generalization of the simple, 1-D results does not appear to be straightforward, and this has thwarted many efforts to extend the method of characteristics to higher dimensions. The characteristic surfaces are significant for theoretical reasons and primarily for the role they play in proving the existence and uniqueness of solutions. The existence and uniqueness theorems are closely related to the concepts of domain of dependence and domain of influence. Integrating along paths on the characteristic surfaces has no advantage over integrating along, say, $\mathbf{x} = $ const paths, which is what is usually done on a computer.

2.2. Riemann invariant manifolds. A different type of wave decomposition occurs when one asks the following question:

Is it possible to find paths in spacetime along which $R_n = $ const?

These paths would be similar to the characteristics in one dimension and could be used as integrating paths. Obviously, these paths are not the bicharacteristics. The paths of interest will have to lie on the surfaces $R_n(t, \mathbf{x}) = $ const. These surfaces can be viewed as Riemann invariant waves and can be used to construct solutions numerically. They are given the name Riemann invariant manifolds (RIM). At first sight, it is not clear why looking for invariants will be useful or whether it is possible to find explicit expressions for their speed and direction of propagation directly from the equations of motion. These matters will be clarified in the end. For now let's find such paths in spacetime, motivated solely by the 1-D implementation of the method of characteristics.

It is easy to see what paths lie on the surfaces $R_n = $ const in spacetime by adding and subtracting the following term in (12):

$$(18) \qquad \mathbf{v}{\cdot}\nabla R_n\ ,$$

where $\mathbf{v}$ is a velocity. Equation (12) is now written

(19) $$\frac{\partial R_n}{\partial t} + (\mathbf{u} + a\mathbf{n} + \mathbf{v}){\cdot}\nabla R_n + aG_n - \mathbf{v}{\cdot}\nabla R_n \;=\; 0\;.$$

If the velocity $\mathbf{v}$ is chosen so that

(20) $$\mathbf{v}{\cdot}\nabla R_n \;=\; aG_n \;=\; a\left[\nabla{\cdot}\mathbf{u} - \mathbf{n}{\cdot}(\nabla\mathbf{u})\,\mathbf{n}\right]\;,$$

then

(21) $$\frac{\partial R_n}{\partial t} + (\mathbf{u} + a\mathbf{n} + \mathbf{v}){\cdot}\nabla R_n \;=\; 0\;.$$

Eq. (21) says that along the paths

(22) $$\dot{\mathbf{x}}(t) = \mathbf{V} \;\equiv\; \mathbf{u} + a\mathbf{n} + \mathbf{v}\;,$$

the function R_n is constant. Equation (20) is simply a compatibility condition, which must be satisfied by the integral curve of (22) in order for it to lie on the surface $R_n = \mathrm{const}$. The velocity $\mathbf{v}$ depends on the local, spatial gradients of the flow, as can be seen from (20). Given a point in the flow where ∇R_n and G_n have a specified value, this relation is linear in the velocity components of $\mathbf{v}$. The reason is that there are an infinity of curves passing through this given point, which lie on the surface $R_n = \mathrm{const}$. All possible choices of $\mathbf{v}$ correspond to all possible directions of motion on this surface. Moreover, it is well known from differential geometry that there are an infinity of curves for every such direction. In what follows, some interesting and useful choices of directions will be examined.

The assumption of zero-entropy gradients allowed the introduction of the Riemann invariants R_n, which simplified the analysis by making the equations integrable. Let's abandon this assumption and repeat the previous analysis. Equation (5) will be the starting point:

$$\left[\frac{\partial p}{\partial t} + (\mathbf{u} + a\mathbf{n}){\cdot}\nabla p\right] + \rho a\mathbf{n}{\cdot}\left[\frac{\partial \mathbf{u}}{\partial t} + (\mathbf{u} + a\mathbf{n}){\cdot}\nabla\mathbf{u}\right]$$
$$+ \rho a^2\left[\nabla{\cdot}\mathbf{u} - \mathbf{n}{\cdot}(\nabla\mathbf{u})\,\mathbf{n}\right] \;=\; 0\;.$$

By adding and subtracting the term

(23) $$\mathbf{v}{\cdot}[\nabla p + \rho a\nabla(\mathbf{u}{\cdot}\mathbf{n})] \;=\; \mathbf{v}{\cdot}\left[\nabla p + \rho a\,(\nabla\mathbf{u})^{\mathrm{T}}\mathbf{n}\right]\;,$$

and for a $\mathbf{v}$ chosen so that

(24) $$\mathbf{v}{\cdot}[\nabla p + \rho a\nabla(\mathbf{u}{\cdot}\mathbf{n})] \;=\; \rho a^2\left[\nabla{\cdot}\mathbf{u} - \mathbf{n}{\cdot}(\nabla\mathbf{u})\,\mathbf{n}\right]\;,$$

one finds

(25) $$\left[\frac{\partial p}{\partial t} + (\mathbf{u} + a\mathbf{n} + \mathbf{v}){\cdot}\nabla p\right] + \rho a\left[\frac{\partial(\mathbf{u}{\cdot}\mathbf{n})}{\partial t} + (\mathbf{u} + a\mathbf{n} + \mathbf{v}){\cdot}\nabla(\mathbf{u}{\cdot}\mathbf{n})\right] \;=\; 0\;.$$

Again $\mathbf{n}$ is assumed to be an arbitrary but fixed unit vector. Equation (25) can be written in a more conventional form as

(26) $$\frac{1}{\rho a}\frac{dp}{dt} + \frac{du_n}{dt} \;=\; 0\;,$$

along the paths

$$\dot{\mathbf{x}}(t) \;=\; \mathbf{V} \;\equiv\; \mathbf{u} + a\mathbf{n} + \mathbf{v}\,, \tag{27}$$

where $u_n \equiv \mathbf{u} \cdot \mathbf{n}$; i.e., the velocity component in the direction of the fixed $\mathbf{n}$ vector. Equation (26) is of the same form as the first of (15), which holds along the C_+ characteristic in the 1-D case. The previous discussion for the $R_n = \text{const}$ surfaces holds for these manifolds as well, but their interpretation is different and more general. The solutions at any two points on such a manifold, connected by a trajectory given by (27), are related in exactly the same way that solutions are related along characteristics in the 1-D case. Knowledge of the integral curves of the vector field (27) allows one to use the simple results of the 1-D theory in multidimensional flows. In what follows, the notation $R_n = \text{const}$ will be used for these manifolds even when entropy gradients are present and the Riemann invariants $R_n = W + \mathbf{u}\cdot\mathbf{n}$ cannot be used.

2.3. Geometry of the Riemann invariant manifolds. It is interesting to see what the geometry of these manifolds is, especially in relation to the characteristic manifolds. A few different ways of describing their geometry are presented in what follows.

One way of visualizing the relative position of the characteristic manifolds and the RIM is by examining the motion of the equivalent $(N-1)$-dimensional fronts. Recall that any surface $\varphi(t, \mathbf{x}) = 0$ in spacetime is equivalent to a wave front. For simplicity consider the case of a 2-D flow; i.e., $N = 2$. Figure 1 shows the local geometry and motion of the wave front $R_n = \text{const}$ for a finite time Δt. The local unit normal of this front is

$$\mathbf{N} \;=\; \frac{\nabla p + \rho a \,(\nabla \mathbf{u})^{\mathrm{T}}\mathbf{n}}{\left|\nabla p + \rho a \,(\nabla \mathbf{u})^{\mathrm{T}}\mathbf{n}\right|}\,. \tag{28}$$

For the case of zero-entropy gradients, this is seen to be

$$\mathbf{N} \;=\; \frac{\nabla R_n}{|\nabla R_n|}\,. \tag{29}$$

It is important to note that the unit normal $\mathbf{n}$ serves as a label for the particular manifold. It determines the fluid velocity component that is used for the equivalent, 1-D problem. The vector $\mathbf{n}$ should be considered as the parameter of the one-parameter family of Riemann invariant wave fronts. From (28), it is apparent that $\mathbf{N}$ depends on $\mathbf{n}$. Moreover, the mapping is not bijective; i.e., it is not always possible to find a wave front $R_n = \text{const}$ for an arbitrary $\mathbf{N}$. The spatial gradients of the flow determine a range of allowed propagation directions $\mathbf{N}$ for these fronts. This is very important, because it is the reason why even a subsonic flow may exhibit locally a "hyperbolic"-type behavior.

It is also useful to define the vector $\mathbf{n}^-$, which determines the front propagating in the $-\mathbf{N}$ direction; i.e.,

$$-\mathbf{N} \;=\; \frac{\nabla p + \rho a \,(\nabla \mathbf{u})^{\mathrm{T}}\mathbf{n}^-}{\left|\nabla p + \rho a \,(\nabla \mathbf{u})^{\mathrm{T}}\mathbf{n}^-\right|}\,, \tag{30}$$
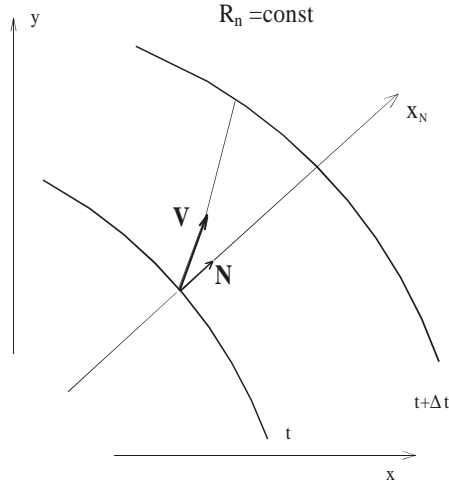
Fig. 1. *Local geometry of the Riemann invariant front $R_n = $ const. The outer normal is $\mathbf{N}$ and its velocity is $\mathbf{V}$.*

if it exists. One can also define $\mathbf{N}^-$ by

$$(31) \qquad \mathbf{N}^- \;=\; \frac{\nabla p - \rho a \,(\nabla \mathbf{u})^{\mathrm{T}} \mathbf{n}}{\left|\nabla p - \rho a \,(\nabla \mathbf{u})^{\mathrm{T}} \mathbf{n}\right|} \;.$$

It is important to keep in mind that in general, $\mathbf{n}^- \neq -\mathbf{n}$ and $\mathbf{N}^- \neq -\mathbf{N}$.

The velocity of the front $R_n = $ const is given by

$$(32) \qquad \mathbf{V} = \mathbf{u} + a\mathbf{n} + \mathbf{v}\;,$$

where $\mathbf{v}$ has to satisfy (24); i.e.,

$$(33) \qquad \mathbf{v}\cdot[\nabla p + \rho a \nabla(\mathbf{u}\cdot\mathbf{n})] \;=\; \rho a^2 \,[\nabla\cdot\mathbf{u} - \mathbf{n}\cdot(\nabla\mathbf{u})\,\mathbf{n}]\;.$$

The geometry of the front at time $t + \Delta t$ is completely determined by the normal front velocity. One can add an arbitrary, tangential velocity component without changing the front geometry. This freedom is seen in choosing the velocity component $\mathbf{v}$, which need only satisfy (33). This equation represents a straight line in velocity space. It is possible to find the front velocity that corresponds to minimum $|\mathbf{v}|$. This is the case when $\mathbf{v} \,/\!/\, \mathbf{N}$. The corresponding front velocity is

$$(34) \qquad \mathbf{V}_H \;=\; \mathbf{u} + a\mathbf{n} + \frac{\rho a^2 \,[\nabla\cdot\mathbf{u} - \mathbf{n}\cdot(\nabla\mathbf{u})\,\mathbf{n}]}{\left|\nabla p + \rho a \,(\nabla\mathbf{u})^{\mathrm{T}}\mathbf{n}\right|}\mathbf{N}\;.$$

The integral curves of this vector field are the curves on the manifold $R_n = $ const, which are closest to the bicharacteristics $\dot{\mathbf{x}}(t) = \mathbf{u} + a\mathbf{n}$. The normal front velocity can be found by combining (28), (32), and (33),

$$(35) \qquad \mathbf{V}_N \;\equiv\; (\mathbf{V}\cdot\mathbf{N})\,\mathbf{N} \;=\; (\mathbf{u}\cdot\mathbf{N})\,\mathbf{N} + \mathcal{M}_n a\mathbf{N}\;,$$

where $\mathcal{M}_n$ is a dimensionless number defined by

$$(36) \qquad \mathcal{M}_n \;\equiv\; \frac{\mathbf{n}\cdot\nabla p + \rho a \nabla\cdot\mathbf{u}}{\left|\nabla p + \rho a \,(\nabla\mathbf{u})^{\mathrm{T}}\mathbf{n}\right|}\;,$$

and plays the role of an algebraic Mach number. The front velocity can also be chosen so that the integral curve of this vector field is as close to the fluid streamline as possible. This is done by minimizing $|a\mathbf{n} + \mathbf{v}|$ in (32). It is possible to show that this is minimized when $(a\mathbf{n} + \mathbf{v}) \mathbin{/\!/} \mathbf{N}$. The front velocity in this case is given by

$$\text{(37)} \qquad\qquad \mathbf{V}_S \;=\; \mathbf{u} + \mathcal{M}_n a \mathbf{N} \;.$$

This particular choice of front velocity is very useful because it resembles the bicharacteristic velocities that generate the characteristic manifolds. It is clear that the parameter $\mathcal{M}_n$ is an indication of how much the manifold $R_n = \text{const}$ deviates from the local characteristic surfaces. The surface $R_n = \text{const}$ is characteristic when $\mathcal{M}_n = \pm 1$. Furthermore, it is time-like when $-1 < \mathcal{M}_n < 1$ and space-like when $|\mathcal{M}_n| > 1$. The following useful relation can be found by combining (28), (33), and (36):

$$\text{(38)} \qquad\qquad \mathcal{M}_n \;=\; \mathbf{n}{\cdot}\mathbf{N} + \frac{\rho a G_n}{\left|\nabla p + \rho a \left(\nabla\mathbf{u}\right)^{\mathrm{T}}\mathbf{n}\right|} \;.$$

Most of the geometrical information of the RIM is contained in the two quantities $\mathbf{N}$ and $\mathcal{M}_n$. They show the allowed direction of propagation of the corresponding fronts and how much they deviate from the characteristic surfaces. They both depend on the unit vector $\mathbf{n}$, i.e., on the particular choice of RIM. Using the definition of $\mathcal{M}_n$ as given in (36) and the equations of motion (1), one can show that

$$\text{(39)} \qquad\qquad \mathcal{M}_n \;\equiv\; \frac{\mathbf{n}{\cdot}\nabla p + \rho a \nabla{\cdot}\mathbf{u}}{\left|\nabla p + \rho a \left(\nabla\mathbf{u}\right)^{\mathrm{T}}\mathbf{n}\right|} \;=\; \frac{\mathbf{n}{\cdot}\nabla p - \dfrac{1}{a}\dfrac{Dp}{Dt}}{\left|\nabla p + \rho a \left(\nabla\mathbf{u}\right)^{\mathrm{T}}\mathbf{n}\right|} \;,$$

where D/Dt denotes the Lagrangian derivative. It is interesting that the magnitude of $\mathcal{M}_n$ depends directly on the difference between the pressure gradient in the $\mathbf{n}$ direction and the pressure change along the fluid-particle streamline. For the case of zero-entropy gradient, it is easy to show that

$$\text{(40)} \qquad\qquad \mathcal{M}_n \;=\; \frac{\mathbf{n}{\cdot}\nabla W + \nabla{\cdot}\mathbf{u}}{\left|\nabla W + \left(\nabla\mathbf{u}\right)^{\mathrm{T}}\mathbf{n}\right|} \;=\; -\frac{1}{a\left|\nabla R_n\right|}\frac{DR_n}{Dt} \;.$$

The starting point of this discussion was (12); i.e.,

$$\text{(41)} \qquad\qquad \frac{\partial R_n}{\partial t} + (\mathbf{u} + a\mathbf{n}){\cdot}\nabla R_n + a\left[\nabla{\cdot}\mathbf{u} - \mathbf{n}{\cdot}(\nabla\mathbf{u})\,\mathbf{n}\right] \;=\; 0 \;,$$

which we write for the special case of zero-entropy gradients for notational convenience only. This equation is a first-order differential equation for the function $R_n = R_n(t, \mathbf{x})$. It resembles a Hamilton–Jacobi equation similar to the one satisfied by the characteristic manifolds. The Hamiltonian in this case is seen to be

$$\text{(42)} \qquad\qquad H\left(\mathbf{x}, \mathbf{p}\right) \;=\; (\mathbf{u} + a\mathbf{n}){\cdot}\mathbf{p} + a G_n \;,$$

where

$$\text{(43)} \qquad\qquad \mathbf{p} \;\equiv\; \nabla R_n \;.$$

The only complication here is that this equation is not independent of the others in the system. Nevertheless, conclusions can be drawn about the geometry of the

integral manifold in $(N+2)$-dimensional space $(t, \mathbf{x}, R_n)$, or more importantly, about the geometry of the slices $R_n = $ const in spacetime $(t, \mathbf{x})$, using the insight gained from the study of first-order PDEs and in particular, the Hamilton–Jacobi equation. If one applies Hamilton–Jacobi theory to (41) formally, then

(44)
$$
\begin{aligned}
\dot{\mathbf{x}}(t) &= \frac{\partial H}{\partial \mathbf{p}} = \mathbf{u} + a\mathbf{n} \,, \\
\dot{\mathbf{p}}(t) &= -\frac{\partial H}{\partial \mathbf{x}} \,, \\
\dot{R}_n(t) &= -aG_n = -a\left[\nabla\!\cdot\!\mathbf{u} - \mathbf{n}\!\cdot\!(\nabla\mathbf{u})\,\mathbf{n}\right] \,.
\end{aligned}
$$

The integral manifold of (41) can be conveniently visualized, locally, as a network of surfaces $R_n = $ const. Equations (44) describe how R_n changes along the bicharacteristic directions $\dot{\mathbf{x}}(t) = \mathbf{u} + a\mathbf{n}$. The bicharacteristic curves do not lie on the surfaces $R_n = $ const. Recall that the vector $\mathbf{n}$ is fixed, which labels the particular network of RIM. If it is possible to find a vector $\mathbf{n}$ such that $G_n = 0$, then the bicharacteristics lie on the surfaces $R_n = $ const. It is important to keep in mind that the integral curves of the vector field $\dot{\mathbf{x}}(t) = \mathbf{u} + a\mathbf{n}$, with $\mathbf{n}$ a fixed vector, are not the bicharacteristics. They are very close to the bicharacteristics for a short time. In order to remain on a bicharacteristic, the vector $\mathbf{n}$ must change according to the second equation of (44).

In general, integrating (44) to find the solution at a point P provides no computational advantage. It is apparent from Figure 2 that there are an infinity of paths C on the surfaces $R_n = $ const that can be used instead. In the present scheme, the problem of finding the solution at P reduces to computing the geometry of the curves accurately, by integrating

(45)
$$
\dot{\mathbf{x}}(t) = \mathbf{V} = \mathbf{u} + a\mathbf{n} + \mathbf{v} \,.
$$

All such paths C are not equivalent numerically. The local curvature of these surfaces is also an important consideration in choosing the most convenient path for numerical integration. One can try to minimize the numerical error by varying the direction of approach to the point P. It is also possible to estimate the curvature of a particular path and to use this information to achieve higher-order accuracy in the integration of (45). Moreover, by varying the vector $\mathbf{n}$, i.e., varying the network of RIM, it is possible to optimize the scheme even further. The algebraic parameter $\mathcal{M}_n$ shows whether the surface $R_n = $ const is space-like or time-like. Surfaces with $\mathcal{M}_n \gg 1$ should be avoided, because the timestep required to integrate (45) accurately would be too restrictive.

It is possible to find the projection of an arbitrary path $\dot{\mathbf{x}}(t) = \mathbf{W}$ on the surface $R_n = $ const. The projection is defined to be the path $\dot{\mathbf{x}}(t) = \mathbf{V}_{\mathrm{w}}$ on $R_n = $ const, such that $\left|\mathbf{v}^{\perp}\right|$ is minimum, where

(46)
$$
\mathbf{v}^{\perp} \equiv \mathbf{V}_{\mathrm{w}} - \mathbf{W} \,.
$$

Since the projection is on the RIM,

(47)
$$
\mathbf{V}_{\mathrm{w}} = \mathbf{u} + a\mathbf{n} + \mathbf{v}_{\mathrm{w}} \,,
$$

where $\mathbf{v}_{\mathrm{w}}$ satisfies the compatibility condition (33). It is straightforward to show that

(48)
$$
\mathbf{v}^{\perp}\!\cdot\!\mathbf{N} = \mathbf{u}\!\cdot\!\mathbf{N} + \mathcal{M}_n a - \mathbf{N}\!\cdot\!\mathbf{W} \,.
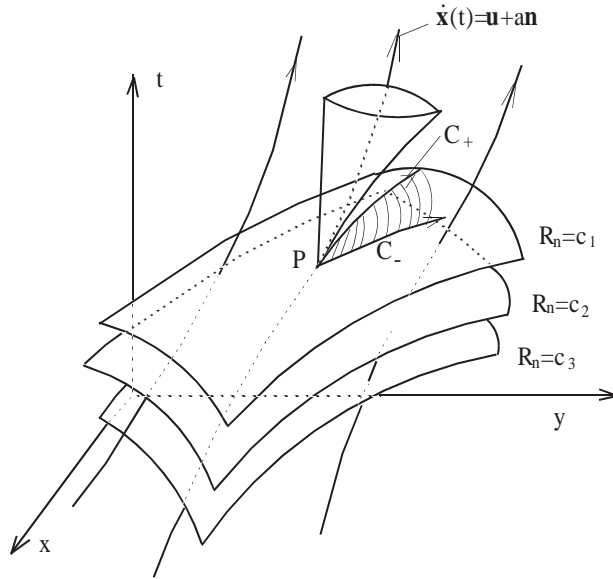$$

FIG. 2. *The projection of the characteristic conoid at P, on the manifold $R_n = c_1$, is shown for the particular case $|\mathcal{M}_n| > 1$. It is contained between the curves C_- and C_+.*

It is seen from (48) that $|\mathbf{v}^\perp|$ is minimum when $\mathbf{v}^\perp \, /\!/ \, \mathbf{N}$. The projection is then

$$(49) \qquad \mathbf{V}_\mathrm{w} \; = \; (\mathbf{u}{\cdot}\mathbf{N} + \mathcal{M}_n a)\,\mathbf{N} + \mathbf{W} - (\mathbf{N}{\cdot}\mathbf{W})\,\mathbf{N} \; .$$

Now, one can find the projection of an arbitrary bicharacteristic direction $\mathbf{u} + a\hat{\mathbf{n}}$, where $\hat{\mathbf{n}}$ is a unit vector. Substituting $\mathbf{W} = \mathbf{u} + a\hat{\mathbf{n}}$ in (49) gives the projection of the bicharacteristic,

$$(50) \qquad \mathbf{V}_p \; = \; \mathbf{u} + \mathcal{M}_n a\mathbf{N} + a\left[\hat{\mathbf{n}} - (\hat{\mathbf{n}}{\cdot}\mathbf{N})\,\mathbf{N}\right] \; .$$

Figure 2 shows the projection of the characteristic conoid on a particular surface $R_n = \mathrm{const}$, which is space-like; i.e., $|\mathcal{M}_n| > 1$. It is reasonable to try to use paths contained in the projected conoid for computational purposes. The paths given by (34) and (37) are in this projection.

Using (50), it is easy to examine the intersection of the manifold $R_n = \mathrm{const}$ and the local characteristic ray cone. This is done by requiring

$$(51) \qquad \mathbf{V}_p \; = \mathbf{u} + a\hat{\mathbf{n}} \; .$$

In other words, the projection vector $\mathbf{V}_p$, tangent to the RIM, is required to be a bicharacteristic vector. From (50) it is seen that one must have

$$(52) \qquad \hat{\mathbf{n}}{\cdot}\mathbf{N} \; = \; \mathcal{M}_n \; .$$

Since $\hat{\mathbf{n}}$ and $\mathbf{N}$ are unit vectors, this equation has a solution only when $-1 \leq \mathcal{M}_n \leq 1$, i.e., when the RIM is time-like or characteristic. This is to be expected because, by definition, a space-like surface element cannot intersect the local characteristic ray cone. It is interesting that when the surface element is not space-like, it is possible to find bicharacteristic directions along which an equivalent, 1-D problem holds. This

situation would be the direct extension of the method of characteristics to multidimensional flows, as it has been attempted in the past. A special solution is the one discussed earlier for the case $\hat{\mathbf{n}} = \mathbf{n}$. In this case (52) reduces to

$$(53) \qquad\qquad \mathbf{n} \cdot \mathbf{N} \;=\; \mathcal{M}_n \;.$$

Using (38),

$$(54) \qquad \mathbf{n} \cdot \mathbf{N} \;=\; \mathcal{M}_n \quad \Rightarrow \quad G_n \;=\; [\nabla \cdot \mathbf{u} - \mathbf{n} \cdot (\nabla \mathbf{u}) \, \mathbf{n}] \;=\; 0 \;.$$

Yet another way to visualize the relative position of the Riemann invariant surfaces and the characteristic manifolds is to examine the cone generated by the vector field (45) in relation to the characteristic ray cone generated by the bicharacteristic vector field. The Riemann invariant cone is generated by varying the unit vector $\mathbf{n}$. It will be different for the different possible choices of $\mathbf{V}$ on each surface $R_n = \text{const}$.

2.4. RIM decomposition. The geometrical picture given above suggests an algorithm for integrating the Euler equations by finding appropriate integration paths in spacetime. The previous analysis can also be viewed in a slightly different way. The original compressible Euler equations have been substituted by the following equivalent system:

$$(55) \qquad \begin{aligned} \frac{\partial R_n}{\partial t} + (\mathbf{u} + \mathcal{M}_n a \mathbf{N}) \cdot \nabla R_n \;&=\; 0 \;, \\[2mm] \frac{\partial R_0}{\partial t} + \mathbf{u} \cdot \nabla R_0 \;&=\; 0 \;, \end{aligned}$$

where

$$\mathcal{M}_n \;=\; \frac{\mathbf{n} \cdot \nabla p + \rho a \nabla \cdot \mathbf{u}}{\left| \nabla p + \rho a \, (\nabla \mathbf{u})^{\mathrm{T}} \mathbf{n} \right|} \;,$$

$$\mathbf{N} \;=\; \frac{\nabla p + \rho a \, (\nabla \mathbf{u})^{\mathrm{T}} \mathbf{n}}{\left| \nabla p + \rho a \, (\nabla \mathbf{u})^{\mathrm{T}} \mathbf{n} \right|} \;,$$

again written for the zero-entropy gradients case for notational convenience only. This is a decomposition into a set of scalar fields, which is different from the characteristic decomposition (14). This decomposition strictly holds when *the spatial gradients are continuous.* This is not as serious a limitation as one might think, at first. The usual characteristic decomposition strictly holds when *the solution is continuous;* i.e., there are no shocks or contact surfaces present. Nevertheless, it is still used in a useful way when shocks are present because it holds on either side where the flow is smooth. The situation is analogous for the RIM decomposition. From a computational point of view one can formally try to discretize these equations in a way that is consistent with a conservative discretization of the original equations, has a prescribed order of accuracy, and does not create spurious oscillations in the presence of discontinuities.

An interesting question to ask is: what new information exists in this decomposition that is not already available in the characteristic decomposition and therefore why would this be useful? From the analysis it can be seen that a great deal more information is contained in the spatial gradients of the flow. The question of asking

whether there are paths along which Riemann invariants exist naturally led to explicit expressions of special combinations of the gradients that are important in finding solutions. It is the combination given in the Mach-like parameter $\mathcal{M}_n$ and unit vector $\mathbf{N}$ that determine speed and direction of propagation of information that is sufficient to determine the solution. Higher-order geometrical quantities, such as local curvature, can also be attained from the equations of motion. It is important to note that the information carried by the RIM waves is not the minimum or in any sense the optimal amount of information needed to generate solutions. It is *sufficient* under the smoothness assumptions. The RIM waves potentially carry more information than the characteristic waves and are free of charge, since one has explicit expressions for their properties directly from the Euler equations, without having to integrate them first. One could try to find contour levels of other quantities that could be used to construct solutions. More often than not, explicit expressions for their geometrical properties cannot be found. Moreover, the RIM decomposition provides more information than what exists in the gradients and could be recovered, say, by a Taylor expansion. This can be seen by looking at the propagation direction $\mathbf{N}$ as a function of the unit vector $\mathbf{n}$. This mapping is not bijective, which means that the range of possible propagation directions may be limited. As $\mathbf{n}$ varies on the unit sphere for 3-D flow, $\mathbf{N}$ does not necessarily attain all values on the unit sphere. This range of directions is given explicitly in the RIM decomposition of the Euler equations if the gradients are known. A Taylor expansion does not give preferred directions.

As an example consider the case of subsonic flow. The local characteristic analysis suggests that information from all possible directions needs to be taken into account to construct a solution. We have an "elliptic"-type behavior. The RIM decomposition and knowledge of the local spatial gradients show whether all this information is really needed. It is possible in some parts of subsonic flow to have *sufficient* information propagating from a particular region of the flow and, thus, have "hyperbolic"-type behavior in subsonic flow. If one likes to think, physically, in terms of characteristic waves, the situation is that the characteristic waves approaching from all possible directions have to combine and interact in such a way that the only information really used is that approaching from the allowed region. Everything else will cancel out. There is no choice under this smoothness assumption. This is a compatibility condition enforced by the Euler equations. Therefore, the RIM decomposition may not always be "better" everywhere in the flow, but it is additional information that can be used to great advantage.

Examining waves of invariants may also be useful for other reasons. It has been noticed that applying boundary conditions on the invariants of the inviscid Euler equations in spectral calculations of the Navier–Stokes equations is the only way to achieve numerical stability. See, e.g., Don and Gottlieb (1990). Although in 1-D flows the characteristic decomposition works well, for multidimensional calculations the RIM decomposition may be the best at boundaries. The RIM decomposition also transforms the problem of integrating the Euler equations into a geometrical problem of integrating paths in spacetime. This is exactly what the method of characteristics achieves in 1-D flow and that is why the RIM decomposition can be considered as the extension of that method to the multidimensional case.

It is also important to notice that the second equation in (55), i.e., the entropy wave equation, is unaffected by the RIM analysis. Entropy waves propagate with the fluid velocity and that does not change. This equation is irrelevant only in the case of homentropic flow as in the 1-D case. In the context of numerical applications this
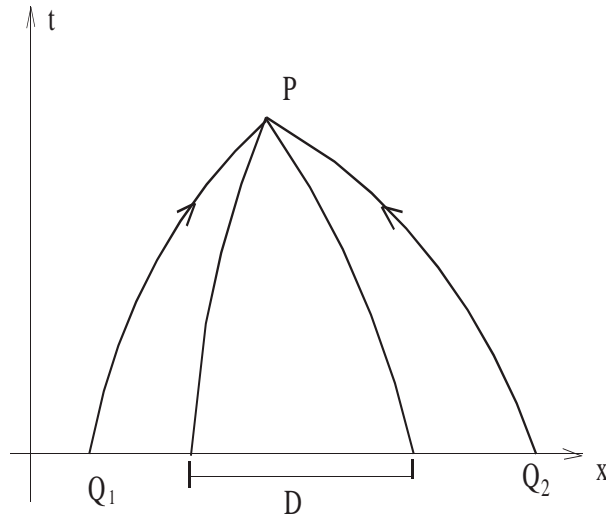
FIG. 3. *The solution at point P is related trivially through the Riemann invariant functions to the solution at points Q_1 and Q_2, which are outside the domain of dependence D.*

means that the RIM analysis does not provide any additional information for this particular equation.

3. RIM and domain of dependence. It is important, at this point, to make some remarks about the information that is provided by the local geometry of these RIM. The fluid velocity $\mathbf{u}$ and the speed of sound a provide information about the local geometry of the characteristic surfaces. In particular, they give the local, bicharacteristic cone. Their interpretation as waves of derivative discontinuities is important. What is more significant is the role they play in proving the existence and uniqueness of solutions. The characteristic surfaces determine the domains of dependence and influence of the solution. The concepts of domains of dependence and influence are a direct result of the assumptions and results of these theorems.

Knowledge of the local, spatial gradients in the flow provides additional information, as seen in the RIM decomposition. It is important to note that the solutions at points on these manifolds are related in a simple way and that these relations can be used to determine the solution at a given point, say, numerically. What may appear disturbing, at first sight, is that these manifolds may be space-like. In other words, the solution at some point may be computed from the data at points outside its domain of dependence. Actually, in the case of zero-entropy gradients, there is a simple, explicit algebraic expression relating points connected by space-like paths in spacetime given by the Riemann invariant $R_n = W + \mathbf{u} \cdot \mathbf{n}$. It then becomes trivial to compute the solution at a given point from the solution at points on these RIM. The difficulty is transferred to the task of finding the exact location of the relevant points by integrating $\dot{\mathbf{x}}(t) = \mathbf{V}$. In any case, no matter what their exact location is, these points are going to be outside the domain of dependence, if the Riemann invariant surface is space-like. There appears to be a disturbing inconsistency with the concept of domain of dependence as described in the uniqueness theorems. Figure 3 is a simplified, 1-D picture illustrating this situation. The solution at point P is computed by using the known solution at points Q_1 and Q_2 outside the domain of dependence D.

Careful examination of the existence and uniqueness theorems for these hyperbolic systems of equations shows that there is really no such inconsistency. It is true that if the data in D are different, then the solution at P will change. But so will the paths Q_1P and Q_2P. What seems odd at first is that even though the data in D are *sufficient* to determine the solution at P, there are points outside D where the data are "related" to the solution at P. The uniqueness statement is that *points outside D cannot affect the solution at P*. This is usually interpreted as meaning that any relation between the data outside D and at P must be completely random, depending on the data on the surface $t = 0$. This is not true. The local, spatial gradients determine a local relation of this form along space-like paths. The data in D are *sufficient* to determine the solution at P, and if the data in D are altered, the solution at P will change. Nevertheless, the solution at P *is not completely unrelated to the data outside D*. This has to do with the fact that knowledge of the local spatial gradients and their smoothness constitutes additional information about how the initial data on $t = 0$ are related. The uniqueness proofs are based on requiring the absolute minimum in terms of smoothness restrictions on the data. The data are simply required to be continuous. Discontinuities in the derivatives are allowed, and it was shown that these discontinuities are propagated by the characteristic surfaces. Other singularities in the derivatives also propagate along the characteristic surfaces. If the data are allowed to have jump discontinuities, then these jumps will propagate along the shock manifolds. The characteristic surfaces separate the regions of spacetime, where the derivatives of the solution are continuous. It is in these regions that knowledge of the gradients provides additional information about the solution. This additional information is conveniently visualized through the geometry of the RIM and can be used for computational purposes.

Those readers familiar with numerical methods for integrating hyperbolic equations are aware of the CFL stability condition which states, in effect, that data outside the domain of dependence must be used to achieve numerical stability. The previous discussion has nothing to do with this notion of numerical stability. Given the smoothness condition, data outside the domain of dependence may be used as prescribed in the RIM decomposition and this has nothing to do with numerics. It suggests an interesting physical relation between the concept of smoothness and that of speed of propagation of information, which is a prevalent concept in modern physics, e.g., in the theory of relativity.

4. Second-order Godunov scheme. A description of an Eulerian MUSCL scheme will be given, since this is the basis for the proposed multidimensional scheme. Most high-order, shock-capturing schemes have been developed using the theory of hyperbolic systems in one space dimension and time. It is therefore convenient to describe the scheme for this special 1-D case and then to show the extension to many spatial dimensions.

The goal is to solve numerically the general, nonlinear system of equations

$$(56) \qquad \frac{\partial U}{\partial t} + \frac{\partial F(U)}{\partial x} = 0 .$$

This is a general conservation law, where t is the time variable, x is the space variable, and $U = U(t, x) \in \Re^M$ is the conserved unknown vector.

A finite-volume formulation is used. The spatial domain is discretized, and the average value of the conserved vector U in the jth cell is denoted by U_j. Quantities associated with the two interfaces of the jth cell are denoted by the subscripts $j \pm 1/2$.

A general conservative scheme is of the form

$$(57) \qquad U_j^{n+1} \;=\; U_j^n - \frac{\Delta t}{\Delta x}\left(\tilde{F}_{j+1/2} - \tilde{F}_{j-1/2}\right) \;.$$

This is really an application of the integral-conservation form of (56) to the jth cell. It gives the cell-averaged, conserved vector U at the time level $n+1$ from the previous time level n. Δx is the size of the cell and Δt is the timestep. The quantities $\tilde{F}_{j\pm1/2}$ are the time-averaged fluxes at the two cell interfaces; i.e.,

$$(58) \qquad \tilde{F}_{j\pm1/2} \;\equiv\; \frac{1}{\Delta t}\int_{t_n}^{t_n+\Delta t} F\left(U_{j\pm1/2}\right) dt \;.$$

It is important to notice that (57) is *exact*. In a numerical scheme it is not possible to calculate the integrals given in (58) exactly. The integrals are therefore approximated, and the final numerical scheme is of the form

$$(59) \qquad U_j^{n+1} \;=\; U_j^n - \frac{\Delta t}{\Delta x}\left(\hat{F}_{j+1/2} - \hat{F}_{j-1/2}\right) \;,$$

where the quantities $\hat{F}_{j\pm1/2}$ are the numerical approximations of the $\tilde{F}_{j\pm1/2}$. Every conservative scheme reduces to calculating the numerical fluxes $\hat{F}_{j\pm1/2}$ at the cell interfaces. All Godunov schemes attempt to compute these fluxes by using the knowledge from the theory of characteristics, locally, at each cell interface. By doing this, the local characteristic wave patterns are accounted for accurately. Since discontinuities are likely to be present, the characteristic problem is generalized to allow for their presence. This constitutes the well-known Riemann problem. How this is done for the case of a second-order Godunov scheme (MUSCL) will now be described.

At any given time t_n, one has only the average values of U in each computational cell, as given by the discrete scheme (59). The first step in calculating the numerical fluxes $\hat{F}_{j\pm1/2}$ is to reconstruct the solution at time t_n by some kind of spatial interpolation. This is a very important step, because the presence of discontinuities in these flows may cause problems. This constitutes the most important step for a variety of high-order, conservative schemes. The second step, then, is to use the knowledge of the solution at this time level to solve a local, characteristic problem in order to calculate the numerical fluxes. These two steps will be given for the MUSCL scheme.

A linear variation of the primitive variables ρ, p, and u is assumed in each cell. The generic quantity q is given by

$$(60) \qquad q\left(x\right) \;=\; q_j + \left(q_x\right)_j \left(x - x_j\right) \;,$$

in the jth cell, where q_j is the average value in the cell, x_j is the center of the cell, and $\left(q_x\right)_j$ is the slope of q in this cell, which is assumed to be constant. Note that discontinuities of these quantities are allowed at the cell interfaces. The slope $\left(q_x\right)_j$ is computed using van Albada's slope limiter; see van Leer (1984).

The numerical fluxes $\hat{F}_{j\pm1/2}$ are calculated by (58) using the trapezoid rule, i.e.,

$$(61) \qquad \hat{F}_{j\pm1/2} \;=\; \frac{1}{2}\left(F\left(U_{j\pm1/2}^n\right) + F\left(U_{j\pm1/2}^{n+1}\right)\right) \;,$$

where the superscript $n+1$ denotes the time level $t_n+\Delta t$. The problem of finding the numerical fluxes becomes that of estimating the solution vector U at the cell interfaces

at times t_n and $t_n + \Delta t$. This procedure ensures second-order accuracy in time. The domain of dependence of $x = x_{j+1/2}$ over the time interval Δt is estimated by the characteristics at the time level t.

For the case of 1-D gas dynamics, the characteristic speeds are given by

$$(62) \qquad c_\pm = u \pm a , \qquad c_0 = u ,$$

where a is the speed of sound. It is known that along the characteristics $C_\pm$ the following differential equations hold:

$$(63) \qquad \left[\frac{\partial p}{\partial t} + (u \pm a)\frac{\partial p}{\partial x} \right] \pm \rho a \left[\frac{\partial u}{\partial t} + (u \pm a)\frac{\partial u}{\partial x} \right] = 0 .$$

These two equations are written in the more conventional form as

$$(64) \qquad \frac{dp}{dt} \pm \rho a \frac{du}{dt} = 0 ,$$

where the time derivatives are derivatives along the appropriate characteristic directions. Along the streamline C_0,

$$(65) \qquad \left[\frac{\partial p}{\partial t} + u\frac{\partial p}{\partial x} \right] - a^2 \left[\frac{\partial \rho}{\partial t} + u\frac{\partial \rho}{\partial x} \right] = 0 ,$$

or

$$(66) \qquad \frac{dp}{dt} - a^2 \frac{d\rho}{dt} = 0 ,$$

which is equivalent to the statement that the entropy remains constant along the streamline. Eqs. (64) and (66) form the basis for the method of characteristics in 1-D gas dynamics. Moreover, when supplemented with the jump conditions, they form the basis for the solution of the 1-D Riemann problem.

The state $U^n_{j+1/2}$ is computed as the solution to the Riemann problem at time t_n. The two initial states are those found by extrapolating the linear interpolants (60) to the interface $j + 1/2$ on either side. The state $U^{n+1}_{j+1/2}$ is a little more complicated. The pressure $p^{n+1}_{j+1/2}$ and velocity $u^{n+1}_{j+1/2}$ are found by solving the Riemann problem with initial states given by the intersection points, $P_\pm$, of the characteristics $C_\pm$ with the x-axis. This is equivalent to discretizing (64) in a way that is consistent with the jump conditions in the presence of a shock.

The density $\rho^{n+1}_{j+1/2}$ is found by discretizing (66) in the following way:

$$(67) \qquad \left(p^{n+1}_{j+1/2} - p_0\right) - a_0^2 \left(\frac{\gamma + 1}{2\gamma} + \frac{\gamma - 1}{2\gamma}\frac{p^{n+1}_{j+1/2}}{p_0} \right) \left(\rho^{n+1}_{j+1/2} - \rho_0\right) = 0$$

if $p^{n+1}_{j+1/2} > p_0$ and

$$(68) \qquad \rho^{n+1}_{j+1/2} = \rho_0 \left(\frac{p^{n+1}_{j+1/2}}{p_0} \right)^{1/\gamma}$$

if $p^{n+1}_{j+1/2} < p_0$. The subscript zero refers to the state found by tracing the streamline back in time. Equation (67) is essentially the jump condition to take care of the

situation where the streamline is being traced through a shock. In the limit of weak shocks this expression gives the density change through an acoustic wave. Equation (68) is just the isentropic relation.

There are many variations of the MUSCL scheme that arise from changing the spatial interpolation scheme or changing the way the states for the Riemann problem are chosen. A different way of picking the two states is by using a Taylor series expansion on either side of the interface $j+1/2$. The left state of the initial condition for the Riemann problem is given by the following expansion about the center of the jth cell:

$$
\begin{aligned}
U_L &= U_j + (x - x_c)\frac{\partial U}{\partial x} + \Delta t\frac{\partial U}{\partial t} \\
&= U_j + (x - x_c)\left(\frac{\partial U}{\partial x}\right) - \Delta t A\left(\frac{\partial U}{\partial x}\right) \\
&= U_j + [(x - x_c)I - \Delta t A]\left(\frac{\partial U}{\partial x}\right) ,
\end{aligned}
$$

(69)

where x_c is the center of the cell, I is the unit matrix, and

(70)
$$
A \equiv \frac{\partial F(U)}{\partial U} .
$$

The spatial derivatives are constant in each cell, since a linear interpolant is used. Similarly, one finds the right state U_R by expanding in the $(j + 1)$th cell. This procedure works in practice, and it is mentioned because it can be extended to the multidimensional case in a straightforward way.

The process of tracing the characteristics back in time is the best way to find the initial condition for the Riemann problem for the 1-D case, but this procedure cannot be extended to the multidimensional case. This is a general problem of all similar methods that use knowledge of the theory of hyperbolic systems in one space dimension to compute numerical fluxes. It is at this point where one can use the theory of RIM to find the states that are connected with an equivalent 1-D characteristic problem.

The conventional way of extending these 1-D schemes to more space dimensions is through Strang-type, dimensional splitting, given in Strang (1968). Each spatial dimension is treated separately, and the result is the "sum" of 1-D problems in the grid directions. Unsplit schemes like that of Colella (1990) use the grid direction to set up a 1-D problem, but the states used as the initial conditions for the Riemann problem are not clearly related via a 1-D problem, even though they are corrected for multidimensional effects. Efforts to create a genuinely multidimensional scheme are those by Roe (1986), Hirsch and Lacor (1989), and Deconinck, Hirsch, and Peuteman (1986). It is also easy to extend the Taylor-series expansion method mentioned earlier to multidimensional flows. The states computed in that way are not clearly related via the 1-D characteristic equations, but the resulting scheme works in practice. Moreover, this scheme is used as a reference point for the multidimensional schemes that are proposed, using the RIM wave decomposition.

Consider now the case of 2-D flow of a perfect gas. The second-order Godunov scheme will be described and used as the starting point for the proposed multidimensional corrections. An orthogonal grid in the x- and y-directions is used. As will be seen later, this restriction on the grid can be dropped when the multidimensional corrections are introduced.

The equations of motion for the 2-D case are

$$(71) \qquad \frac{\partial U}{\partial t} + \frac{\partial F_x(U)}{\partial x} + \frac{\partial F_y(U)}{\partial y} = 0 ,$$

where

$$(72) \qquad U = \begin{pmatrix} \rho \\ \rho u \\ \rho v \\ \rho e_t \end{pmatrix}, \quad F_x(U) = \begin{pmatrix} \rho u \\ p + \rho u^2 \\ \rho u v \\ \rho u e_t + p u \end{pmatrix}, \quad F_y(U) = \begin{pmatrix} \rho v \\ \rho u v \\ p + \rho v^2 \\ \rho v e_t + p v \end{pmatrix} .$$

$\mathbf{u} = (u, v)^{\mathrm{T}}$ is the 2-D, velocity vector, and $e_t = e + \frac{1}{2}|\mathbf{u}|^2$ is the total energy. The internal energy e is related to the pressure p by the perfect gas equation of state.

The spatial-interpolation scheme is the 1-D scheme given by (60) and is implemented in the two orthogonal grid directions. As mentioned earlier, the spatial-interpolation scheme is a very important step but is independent of the efforts to correct for multidimensional effects in the time integration. One can devise higher-order interpolation schemes, which take into account the presence of discontinuities, such as the interpolation used in ENO schemes; see Harten et al. (1987). It is also possible to devise schemes that work on unstructured grids. At any given time, knowledge of the spatial gradients of the flow will be assumed in using the theory of RIM to develop a multidimensional scheme.

A Riemann problem is solved at each interface to determine the states at the time level $t_n + \Delta t$. The two states that are used as the initial condition for the Riemann problem at the interface $(i + 1/2, j)$ are given by the Taylor-series expansions on either side of the interface. The left state is given by expanding about the center of the (i, j)th cell to the center of the interface, $\mathbf{x}_p$, at the later time $t + \Delta t$. It is easy to see that the extension of (69) to the 2-D case is

$$(73) \qquad U_L = U_{ij} + [(\mathbf{x}_p - \mathbf{x}_c) I - \Delta t \mathbf{A}] \cdot \nabla U ,$$

where $\mathbf{x}_c$ is the center of the cell, I is the unit matrix, and

$$(74) \qquad \mathbf{A} \equiv (A_x, A_y)^{\mathrm{T}} = \left(\frac{\partial F_x(U)}{\partial U}, \frac{\partial F_y(U)}{\partial U} \right)^{\mathrm{T}} .$$

It is more convenient to expand the primitive variables ρ, p, and $\mathbf{u}$ instead of the conserved vector U. The left state, is then given by

$$(75) \qquad \rho_L = \rho + [(\mathbf{x}_p - \mathbf{x}_c) - \mathbf{u}\Delta t] \cdot \nabla \rho - \Delta t \rho \nabla \cdot \mathbf{u} ,$$

$$(76) \qquad p_L = p + [(\mathbf{x}_p - \mathbf{x}_c) - \mathbf{u}\Delta t] \cdot \nabla p - \Delta t \rho a^2 \nabla \cdot \mathbf{u} ,$$

$$(77) \qquad \mathbf{u}_L = \mathbf{u} + [(\mathbf{x}_p - \mathbf{x}_c) - \mathbf{u}\Delta t] \cdot \nabla \mathbf{u} - \Delta t \frac{1}{\rho} \nabla p ,$$

where all quantities are evaluated at the center of the (i, j)th cell. Similarly, one can find the right state by Taylor expanding about the center of the $(i + 1, j)$th cell. The velocity component normal to the interface, i.e., $\mathbf{u}_L \cdot \mathbf{N}_s$, is used as the left scalar velocity for the 1-D Riemann problem. In other words, a 1-D Riemann

problem is solved in the direction of the grid line, using the above left and right states. As mentioned earlier, these states are not clearly related by the 1-D characteristic equations even in smooth, shock-free flow. The tangential velocity component used to compute the numerical fluxes at the interface is $\mathbf{u}_L \cdot \mathbf{N}_s^\perp$, if $\mathbf{u}_L \cdot \mathbf{N}_s > 0$; otherwise it is $\mathbf{u}_R \cdot \mathbf{N}_s^\perp$. The notation

$$(78) \qquad \mathbf{a}^\perp \equiv (\hat{e}_x \times \hat{e}_y) \times \mathbf{a},$$

for an arbitrary, 2-D vector $\mathbf{a}$, will be used throughout. $\mathbf{a}^\perp$ is just $\mathbf{a}$, rotated by $90°$.

5. Multidimensional, second-order Godunov scheme. From the theory of RIM it is seen that the original compressible Euler equations can be substituted by the equivalent system given by (55). This is a decomposition into a set of scalar fields, which is different from the characteristic decomposition. From a computational point of view one can formally try to discretize these equations in a way that is consistent with a conservative discretization of the original equations, has a prescribed order of accuracy, and does not create spurious oscillations in the presence of discontinuities.

In the following numerical application it is proposed to use the RIM that pass through the interface of each computational cell to find the states that are clearly related through an equivalent 1-D, characteristic problem. As a first step, the geometry of the RIM $R_n = $ const, corresponding to the arbitrary unit vector $\mathbf{n}$, will be examined in the vicinity of the computational cell (i, j). The spatial gradients are assumed to be known from the spatial-interpolation scheme. Moreover, the spatial gradients are constant in each cell, since a linear interpolation is used. The unit normal $\mathbf{N}$ and the algebraic normal Mach number $\mathcal{M}_n$ of the 2-D front $R_n = $ const are given by

$$(79) \qquad \mathbf{N} = \frac{\nabla p + \rho a \left(\nabla \mathbf{u}\right)^{\mathrm{T}} \mathbf{n}}{\left|\nabla p + \rho a \left(\nabla \mathbf{u}\right)^{\mathrm{T}} \mathbf{n}\right|},$$

$$(80) \qquad \mathcal{M}_n \equiv \frac{\mathbf{n} \cdot \nabla p + \rho a \nabla \cdot \mathbf{u}}{\left|\nabla p + \rho a \left(\nabla \mathbf{u}\right)^{\mathrm{T}} \mathbf{n}\right|}.$$

Both quantities are assumed constant in each computational cell. An arbitrary direction on the manifold $R_n = $ const is given by

$$(81) \qquad \dot{\mathbf{x}}_n(t) = \mathbf{u} + a\nu,$$

where

$$(82) \qquad \nu \equiv \mathcal{M}_n \mathbf{N} + \mathcal{M}_t \mathbf{N}^\perp.$$

$\mathcal{M}_t$ is unspecified and it reflects the infinity of paths on this particular manifold. The Mach number of a particular trajectory $\dot{\mathbf{x}}_n(t)$ is

$$(83) \qquad \mathcal{M} \equiv |\nu| = \sqrt{\mathcal{M}_n^2 + \mathcal{M}_t^2} > 0.$$

This positive number $\mathcal{M}$ contains the information about the relative position of the corresponding trajectory and the bicharacteristic conoid. When $\mathcal{M} = 1$, the path is tangent to the bicharacteristic cone. When $\mathcal{M} < 1$, it is time-like, and when $\mathcal{M} > 1$, it is space-like.

The solution is known at time t. From the knowledge of the spatial gradients of the flow it is possible to find, approximately, all paths on the manifold $R_n = $ const,

which pass through the center of the interface $(i + 1/2, j)$ at time $t + \Delta t$. These paths must be such that

$$(84) \quad \mathbf{x}_p \;=\; \mathbf{x}_n(t + \Delta t) \;=\; \mathbf{x}_n(t) + \int_t^{t+\Delta t} \left[\mathbf{u}(\tau, \mathbf{x}_n(\tau)) + a(\tau, \mathbf{x}_n(\tau))\nu(\tau, \mathbf{x}_n(\tau)) \right] d\tau \;.$$

By approximating these paths by straight lines in time, one finds

$$(85) \quad \mathbf{x}_p \;\approx\; \mathbf{x}_w + \Delta t \left[\mathbf{u}(t, \mathbf{x}_w) + a(t, \mathbf{x}_w)\nu(t, \mathbf{x}_w) \right] \;,$$

where $\mathbf{x}_w \equiv \mathbf{x}_n(t)$. Using the linear interpolants for the velocity $\mathbf{u}$ and the speed of sound a at time t and the fact that ν is constant in each cell,

$$(86) \quad \mathbf{x}_p - \mathbf{x}_w \;\approx\; \Delta t \left\{ \mathbf{u} + (\mathbf{x}_w - \mathbf{x}_c)\cdot\nabla\mathbf{u} + \left[a + (\mathbf{x}_w - \mathbf{x}_c)\cdot\nabla a \right] \nu \right\} \;,$$

where all quantities are now evaluated at the center of the cell. Eq. (86) can be used to solve for $\mathbf{x}_w$ as a function of $\mathcal{M}_t$. It can be written as

$$(87) \quad \left[I + \Delta t \left(\nabla\mathbf{u} + \nu\nabla a \right) \right] (\mathbf{x}_w - \mathbf{x}_c) \;\approx\; \mathbf{x}_p - \mathbf{x}_c - \Delta t \left(\mathbf{u} + a\nu \right) \;.$$

Equation (87) is a linear system in the unknown vector $\mathbf{x}_w - \mathbf{x}_c$. The determinant of this system is easily found to be

$$(88) \quad \begin{aligned} D \;&=\; 1 + \Delta t \left(\nabla\cdot\mathbf{u} \right) + \Delta t^2 \det\left(\nabla\mathbf{u} \right) + \Delta t\, \nu\cdot\left[I + \Delta t \widehat{(\nabla\mathbf{u})} \right] \nabla a \\ &=\; 1 + \Delta t \left(\nabla\cdot\mathbf{u} + \nu\cdot\nabla a \right) + \Delta t^2 \left[\det\left(\nabla\mathbf{u} \right) + \nu\cdot\widehat{(\nabla\mathbf{u})}\nabla a \right] \;. \end{aligned}$$

For small enough timestep Δt, $D \approx 1$. Equation (87) can be solved to give

$$(89) \quad \mathbf{x}_p - \mathbf{x}_w \;=\; (1 - 1/D)\,\Delta\mathbf{x}_p + \frac{\Delta t}{D}\left[\mathbf{u} - \widetilde{(\nabla\mathbf{u})}\left(\Delta\mathbf{x}_p - \Delta t\mathbf{u} \right) \right] + \frac{\Delta t}{D}a\hat{T}\nu \;,$$

where $\Delta\mathbf{x}_p \equiv \mathbf{x}_p - \mathbf{x}_c$, $a\hat{T}$ is the tensor

$$(90) \quad a\hat{T} \;\equiv\; aI + (\nabla a)^\perp (\Delta\mathbf{x}_p)^\perp + \Delta t \left[a\widetilde{(\nabla\mathbf{u})} - (\nabla a)^\perp \mathbf{u}^\perp \right] \;,$$

and

$$(91) \quad \widehat{(\nabla\mathbf{u})} \;\equiv\; \begin{pmatrix} \dfrac{\partial v}{\partial y} & \dfrac{\partial v}{\partial x} \\[2mm] \dfrac{\partial u}{\partial y} & \dfrac{\partial u}{\partial x} \end{pmatrix}, \quad \widetilde{(\nabla\mathbf{u})} \;\equiv\; \begin{pmatrix} \dfrac{\partial v}{\partial y} & -\dfrac{\partial u}{\partial y} \\[2mm] -\dfrac{\partial v}{\partial x} & \dfrac{\partial u}{\partial x} \end{pmatrix}.$$

Equation (89) gives $\mathbf{x}_w$ as a function of $\mathcal{M}_t$, which is contained in ν. In other words, it is the locus of all points, at time t, that are connected with point $(t + \Delta t, \mathbf{x}_p)$ by the 1-D characteristic differential equation

$$(92) \quad \frac{dp}{dt} + \rho a \frac{du_n}{dt} \;=\; 0 \;,$$

where $u_n = \mathbf{u}\cdot\mathbf{n}$, for the particular choice of $\mathbf{n}$ (see Figure 4).

For the point $\mathbf{x}_w$ to be inside the cell (i, j), the following relations must hold:

$$(93) \quad \begin{aligned} 0 \;&<\; (\mathbf{x}_p - \mathbf{x}_w)\cdot\mathbf{N}_s \;<\; \Delta x \;, \\ \left| (\mathbf{x}_p - \mathbf{x}_w)\cdot\mathbf{N}_s^\perp \right| \;&<\; 0.5\Delta y \;, \end{aligned}$$
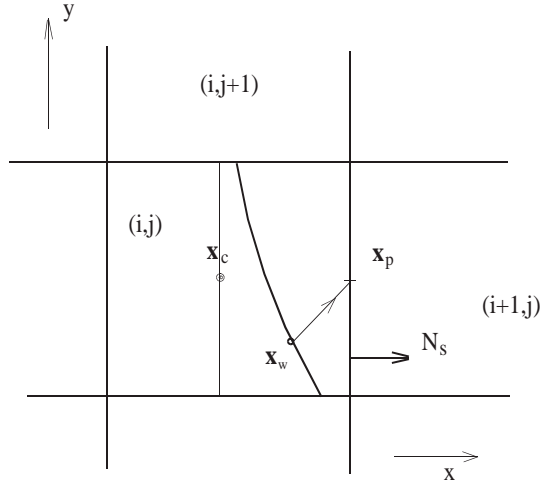
FIG. 4. *The locus of all points* $\mathbf{x}_w$ *in the cell* (i,j) *at time t, which are connected with point* $(t+\Delta t, \mathbf{x}_p)$ *by the* 1-*D characteristic differential equation* (92).

where $(\Delta x, \Delta y)$ is the size of the cell. If the point $\mathbf{x}_w$ is restricted to the half of the cell closest to the interface $(i+1/2, j)$, then

(94)
$$0 \;<\; (\mathbf{x}_p - \mathbf{x}_w){\cdot}\mathbf{N}_s \;<\; 0.5\Delta x \;,$$
$$\left|(\mathbf{x}_p - \mathbf{x}_w){\cdot}\mathbf{N}_s^{\perp}\right| \;<\; 0.5\Delta y \;.$$

Equation (89) can be used to find the range of the parameter $\mathcal{M}_t$ for which the inequalities (93) and (94) hold. This range can be found explicitly if the simplifying assumption $D \approx 1$ is made. In that case, (89) becomes

(95)
$$\frac{\mathbf{x}_p - \mathbf{x}_w}{\Delta t} \;\approx\; \mathbf{V}_c + a\hat{T}\nu \;,$$

where

(96)
$$\mathbf{V}_c \;\equiv\; \mathbf{u} - \widetilde{(\nabla \mathbf{u})}\left(\Delta \mathbf{x}_p - \Delta t \mathbf{u}\right) \;.$$

The inequalities (94) can now be written

(97)
$$0 \;<\; u_s \;<\; 0.5\frac{\Delta x}{\Delta t} \;\equiv\; 0.5 u_g \;,$$
$$|v_s| \;<\; 0.5\frac{\Delta y}{\Delta t} \;\equiv\; 0.5 v_g \;,$$

where

(98)
$$u_s \;\equiv\; \frac{\mathbf{x}_p - \mathbf{x}_w}{\Delta t}{\cdot}\mathbf{N}_s \;=\; \mathbf{V}_c{\cdot}\mathbf{N}_s + a\nu{\cdot}\left(\hat{T}^{\mathrm{T}}\mathbf{N}_s\right) \;,$$
$$v_s \;\equiv\; \frac{\mathbf{x}_p - \mathbf{x}_w}{\Delta t}{\cdot}\mathbf{N}_s^{\perp} \;=\; \mathbf{V}_c{\cdot}\mathbf{N}_s^{\perp} + a\nu{\cdot}\left(\hat{T}^{\mathrm{T}}\mathbf{N}_s^{\perp}\right) \;.$$

Using (82), the inequalities (97) become

(99)
$$0 \;<\; \mathbf{V}_c{\cdot}\mathbf{N}_s + a\mathcal{M}_n\mathbf{N}{\cdot}\mathbf{k}_s - a\mathcal{M}_t\mathbf{N}{\cdot}\mathbf{k}_s^{\perp} \;<\; 0.5 u_g \;,$$
$$-0.5 v_g \;<\; \mathbf{V}_c{\cdot}\mathbf{N}_s^{\perp} + a\mathcal{M}_n\mathbf{N}{\cdot}\kappa_s - a\mathcal{M}_t\mathbf{N}{\cdot}\kappa_s^{\perp} \;<\; 0.5 v_g \;,$$

where

(100)
$$\mathbf{k}_s \; \equiv \; \hat{T}^{\mathrm{T}} \mathbf{N}_s \;, \qquad \kappa_s \; \equiv \; \hat{T}^{\mathrm{T}} \mathbf{N}_s^\perp \;.$$

This can be written as

(101)
$$\mathbf{V}_c{\cdot}\mathbf{N}_s + a\mathcal{M}_n\mathbf{N}{\cdot}\mathbf{k}_s - 0.5u_g \; < \; a\mathcal{M}_t\mathbf{N}{\cdot}\mathbf{k}_s^\perp \; < \; \mathbf{V}_c{\cdot}\mathbf{N}_s + a\mathcal{M}_n\mathbf{N}{\cdot}\mathbf{k}_s \;,$$
$$\mathbf{V}_c{\cdot}\mathbf{N}_s^\perp + a\mathcal{M}_n\mathbf{N}{\cdot}\kappa_s - 0.5v_g \; < \; a\mathcal{M}_t\mathbf{N}{\cdot}\kappa_s^\perp \; < \; \mathbf{V}_c{\cdot}\mathbf{N}_s^\perp + a\mathcal{M}_n\mathbf{N}{\cdot}\kappa_s + 0.5v_g \;.$$

This is equivalent to

(102)
$$\mathcal{M}_t \in (\alpha_-, \alpha_+) \cap (\beta_-, \beta_+) \;,$$

where

(103)
$$\alpha_\pm \; \equiv \; \begin{smallmatrix}\max\\\min\end{smallmatrix} \left(\frac{\mathbf{V}_c{\cdot}\mathbf{N}_s + a\mathcal{M}_n\mathbf{N}{\cdot}\mathbf{k}_s - 0.5u_g}{a\mathbf{N}{\cdot}\mathbf{k}_s^\perp} \;,\; \frac{\mathbf{V}_c{\cdot}\mathbf{N}_s + a\mathcal{M}_n\mathbf{N}{\cdot}\mathbf{k}_s}{a\mathbf{N}{\cdot}\mathbf{k}_s^\perp} \right),$$
$$\beta_\pm \; \equiv \; \begin{smallmatrix}\max\\\min\end{smallmatrix} \left(\frac{\mathbf{V}_c{\cdot}\mathbf{N}_s^\perp + a\mathcal{M}_n\mathbf{N}{\cdot}\kappa_s - 0.5v_g}{a\mathbf{N}{\cdot}\kappa_s^\perp} \;,\; \frac{\mathbf{V}_c{\cdot}\mathbf{N}_s^\perp + a\mathcal{M}_n\mathbf{N}{\cdot}\kappa_s + 0.5v_g}{a\mathbf{N}{\cdot}\kappa_s^\perp} \right) \;.$$

Define

(104)
$$\mathcal{M}_t^\pm \; \equiv \; \begin{smallmatrix}\min\\\max\end{smallmatrix} (\alpha_\pm, \beta_\pm) \;.$$

If $\mathcal{M}_t^- > \mathcal{M}_t^+$, then there is no solution to these inequalities. Otherwise, the inequalities are satisfied for

(105)
$$\mathcal{M}_t \in \left(\mathcal{M}_t^-, \mathcal{M}_t^+ \right) \;.$$

This range of values can be restricted further, if one requires that

(106)
$$\mathcal{M} \; = \; \sqrt{\mathcal{M}_n^2 + \mathcal{M}_t^2} \; \leq \; \mathcal{M}_{\max} \;.$$

This restricts the locus of points to those within a certain distance from the domain of dependence of the point $(t + \Delta t, \mathbf{x}_p)$.

It is now a straightforward calculation to find the pressure, density, and velocity at the point $\mathbf{x}_w$, using the linear interpolants in the (i,j)th cell. We denote this state with the superscript W. The pressure at point $(t, \mathbf{x}_w)$ is given by

(107)
$$p^W \; = \; p + (\mathbf{x}_w - \mathbf{x}_c){\cdot}\nabla p \;.$$

By substituting $\mathbf{x}_w$ from (89), one finds

(108)
$$\begin{aligned} p^W \; &= \; p^G - a\left[\nu{\cdot}\nabla p - \rho a \nabla{\cdot}\mathbf{u}\right]\Delta t - (1 - 1/D)\Delta\mathbf{x}_p{\cdot}\nabla p \\ &\quad - \Delta t \left[\mathbf{E}_\nu^{(1)} - (1 - 1/D)\left(\mathbf{u} + a\nu\right)\right]{\cdot}\nabla p - \Delta t^2\, \mathbf{E}_\nu^{(2)}{\cdot}\nabla p \;, \end{aligned}$$

where p^G is the pressure given by the conventional Godunov scheme in (76); i.e.,

(109)
$$p^G \; = \; p + \left[(\mathbf{x}_p - \mathbf{x}_c) - \Delta t \mathbf{u}\right]{\cdot}\nabla p - \Delta t \rho a^2 \nabla{\cdot}\mathbf{u} \;.$$

All quantities are evaluated at the center of the cell, and the two vectors $\mathbf{E}_\nu^{(1)}$ and $\mathbf{E}_\nu^{(2)}$ are given by

$$(110) \qquad \mathbf{E}_\nu^{(1)} \;\equiv\; \frac{1}{D}\left[\left(\nu\cdot\Delta\mathbf{x}_p^\perp\right)(\nabla a)^\perp - \widetilde{(\nabla\mathbf{u})}\Delta\mathbf{x}_p\right]\;,$$

$$(111) \qquad \mathbf{E}_\nu^{(2)} \;\equiv\; \frac{1}{D}\left[\widetilde{(\nabla\mathbf{u})}\left(\mathbf{u}+a\nu\right) - \left(\nu\cdot\mathbf{u}^\perp\right)(\nabla a)^\perp\right]\;.$$

Similarly, for the component of the velocity vector in the $\mathbf{n}$ direction, one can show that

$$(112) \qquad \begin{aligned} \mathbf{u}^W\cdot\mathbf{n} &= \mathbf{u}^G\cdot\mathbf{n} + \left[\frac{1}{\rho}\mathbf{n}\cdot\nabla p - a\nu\cdot(\nabla\mathbf{u})^{\mathrm{T}}\mathbf{n}\right] - (1-1/D)\Delta\mathbf{x}_p\cdot(\nabla\mathbf{u})^{\mathrm{T}}\mathbf{n} \\ &\quad - \Delta t\,[\mathbf{E}_\nu^{(1)} - (1-1/D)\,(\mathbf{u}+a\nu)]\cdot(\nabla\mathbf{u})^{\mathrm{T}}\mathbf{n} - \Delta t^2\,\mathbf{E}_\nu^{(2)}\cdot(\nabla\mathbf{u})^{\mathrm{T}}\mathbf{n}\;. \end{aligned}$$

By the definition of the RIM,

$$(113) \qquad \nu\cdot\left[\nabla p + \rho a\,(\nabla\mathbf{u})^{\mathrm{T}}\mathbf{n}\right] \;=\; \mathbf{n}\cdot\nabla p + \rho a\nabla\cdot\mathbf{u}\;.$$

Therefore, (112) can be written

$$(114) \qquad \begin{aligned} \mathbf{u}^W\cdot\mathbf{n} &= \mathbf{u}^G\cdot\mathbf{n} + \frac{1}{\rho}\left[\nu\cdot\nabla p - \rho a\nabla\cdot\mathbf{u}\right]\Delta t - (1-1/D)\Delta\mathbf{x}_p\cdot(\nabla\mathbf{u})^{\mathrm{T}}\mathbf{n} \\ &\quad - \Delta t\,[\mathbf{E}_\nu^{(1)} - (1-1/D)\,(\mathbf{u}+a\nu)]\cdot(\nabla\mathbf{u})^{\mathrm{T}}\mathbf{n} - \Delta t^2\,\mathbf{E}_\nu^{(2)}\cdot(\nabla\mathbf{u})^{\mathrm{T}}\mathbf{n}\;. \end{aligned}$$

It is seen from these equations that the leading order difference between the state given by the Godunov scheme and the state given by the RIM is the term

$$(115) \qquad \nu\cdot\nabla p - \rho a\nabla\cdot\mathbf{u}\;,$$

for both the pressure and the velocity. The density is given by a similar equation,

$$(116) \qquad \begin{aligned} \rho^W &= \rho^G - [a\nu\cdot\nabla\rho - \rho\nabla\cdot\mathbf{u}]\,\Delta t - (1-1/D)\Delta\mathbf{x}_p\cdot\nabla\rho \\ &\quad - \Delta t\,[\mathbf{E}_\nu^{(1)} - (1-1/D)\,(\mathbf{u}+a\nu)]\cdot\nabla\rho - \Delta t^2\,\mathbf{E}_\nu^{(2)}\cdot\nabla\rho\;. \end{aligned}$$

The state computed this way, i.e., by tracing the RIM $R_n = \text{const}$, serves as the left state for a 1-D characteristic problem. To find the right state, one needs to trace the $R_{-n} = \text{const}$ manifold, which corresponds to the unit vector $-\mathbf{n}$. A locus of points $(t, \mathbf{x}_w)$ can be found, which are connected with the point $(t+\Delta t, \mathbf{x}_p)$ by

$$(117) \qquad \frac{dp}{dt} - \rho a\frac{du_n}{dt} \;=\; 0\;.$$

These points may lie in the (i,j)th cell or the $(i+1,j)$th cell or both, depending on the local flow gradients. The solution to this 1-D characteristic problem will give the pressure and velocity component $\mathbf{u}\cdot\mathbf{n}$ at the point $(t+\Delta t, \mathbf{x}_p)$.

The density is found by tracing the streamline back in time in a way completely analogous to the way the Riemann invariant paths were traced. The density is computed using (67) and (68) as in the 1-D algorithm. This is because the states along the streamline are connected with the 1-D characteristic equation (66) even in the general multidimensional case.

It is obvious that the velocity component $\mathbf{u} \cdot \mathbf{n}^\perp$ is also needed. There are two ways to find this. One way is to examine the geometry of the RIM that correspond to the unit vectors $\pm \mathbf{n}^\perp$ and to set up another 1-D characteristic problem. There is also a different way of calculating the velocity component $\mathbf{u} \cdot \mathbf{n}^\perp$, which is now described. The momentum equation is

$$(118) \qquad \frac{\partial \mathbf{u}}{\partial t} + \mathbf{u} \cdot \nabla \mathbf{u} + \frac{1}{\rho} \nabla p = 0 .$$

By taking the inner product of this equation with the unit vector $\mathbf{n}^\perp$, one finds

$$(119) \qquad \frac{\partial}{\partial t} \left(\mathbf{u} \cdot \mathbf{n}^\perp \right) + \mathbf{u} \cdot (\nabla \mathbf{u})^\mathrm{T} \mathbf{n}^\perp + \frac{1}{\rho} \mathbf{n}^\perp \cdot \nabla p = 0 .$$

It can be seen that along any path $\dot{\mathbf{x}}(t) = \mathbf{u} + a\nu_u$ in spacetime such that

$$(120) \qquad \nu_u \cdot (\nabla \mathbf{u})^\mathrm{T} \mathbf{n}^\perp = \frac{1}{\rho a} \mathbf{n}^\perp \cdot \nabla p ,$$

one has

$$(121) \qquad \frac{\partial}{\partial t} \left(\mathbf{u} \cdot \mathbf{n}^\perp \right) + (\mathbf{u} + a\nu_u) \cdot \nabla \left(\mathbf{u} \cdot \mathbf{n}^\perp \right) = 0 ,$$

which means that the velocity component $\mathbf{u} \cdot \mathbf{n}^\perp$ is constant along this path. In effect, a manifold is defined in a way completely analogous to the RIM. It is straightforward to show that (120) implies that

$$(122) \qquad \nu_u = \zeta_n \mathbf{N}_u + \zeta_t \mathbf{N}_u^\perp ,$$

where

$$(123) \qquad \mathbf{N}_u = \frac{(\nabla \mathbf{u})^\mathrm{T} \mathbf{n}^\perp}{\left| (\nabla \mathbf{u})^\mathrm{T} \mathbf{n}^\perp \right|} ,$$

$$(124) \qquad \zeta_n = \frac{1}{\rho a} \frac{\mathbf{n}^\perp \cdot \nabla p}{\left| (\nabla \mathbf{u})^\mathrm{T} \mathbf{n}^\perp \right|} .$$

The equations for this manifold are the same as those for the RIM with the following substitutions:

$$(125) \qquad \mathbf{N} \to \mathbf{N}_u , \quad \mathcal{M}_n \to \zeta_n, \quad \text{and} \quad \mathcal{M}_t \to \zeta_t .$$

One can find a locus of points in a given cell by tracing this manifold back in time, exactly the way the RIM were traced. It can be seen, then, that the velocity component $\mathbf{u} \cdot \mathbf{n}^\perp$ is given by

$$(126) \qquad \begin{aligned} \mathbf{u}^W \cdot \mathbf{n}^\perp &= \mathbf{u}^G \cdot \mathbf{n}^\perp - (1 - 1/D_u) \Delta \mathbf{x}_p \cdot (\nabla \mathbf{u})^\mathrm{T} \mathbf{n}^\perp - \Delta t^2 \, \mathbf{E}_{\nu_u}^{(2)} \cdot (\nabla \mathbf{u})^\mathrm{T} \mathbf{n}^\perp \\ &\quad - \Delta t \left[\mathbf{E}_{\nu_u}^{(1)} - (1 - 1/D_u) (\mathbf{u} + a\nu_u) \right] \cdot (\nabla \mathbf{u})^\mathrm{T} \mathbf{n}^\perp , \end{aligned}$$

where

$$(127) \qquad D_u \; \equiv \; 1 + \Delta t \left(\nabla\cdot\mathbf{u} + \nu_u\cdot\nabla a \right) + \Delta t^2 \left[\det\left(\nabla\mathbf{u} \right) + \nu_u\cdot\widehat{(\nabla\mathbf{u})}\nabla a \right] \; ,$$

$$(128) \qquad \mathbf{E}^{(1)}_{\nu_u} \; \equiv \; \frac{1}{D_u} \left[\left(\nu_u\cdot\Delta\mathbf{x}_p^{\perp} \right) \left(\nabla a \right)^{\perp} - \widetilde{(\nabla\mathbf{u})}\Delta\mathbf{x}_p \right] \; ,$$

$$(129) \qquad \mathbf{E}^{(2)}_{\nu_u} \; \equiv \; \frac{1}{D_u} \left[\widetilde{(\nabla\mathbf{u})} \left(\mathbf{u} + a\nu_u \right) - \left(\nu_u\cdot\mathbf{u}^{\perp} \right) \left(\nabla a \right)^{\perp} \right] \; .$$

The theory of RIM has given us a way of finding a 1-D characteristic problem near the interface $(i + 1/2, j)$. The solution of the 1-D problem gives us the state at $(t + \Delta t, \mathbf{x}_p)$ and hence the numerical fluxes. In the procedure described, the unit vector $\mathbf{n}$ was arbitrary. Therefore, the derived equations give us a two-parameter family of schemes for computing the fluxes. One degree of freedom comes from $\mathbf{n}$ and the other from the freedom to choose $\mathcal{M}_t$, although the latter is restricted by relations like (105). This family of schemes is consistent with the multidimensional theory and provides a way for correcting the conventional Godunov scheme. The conventional scheme assumes $\mathbf{n} = \mathbf{N}_s$; i.e., it sets up a 1-D problem in the grid direction. If this choice is made, then one is left with choosing $\mathcal{M}_t$ in each case. The conventional scheme based on the Taylor-series extrapolation always takes the left state from the cell (i, j) and the right state from the cell $(i + 1, j)$. The proposed multidimensional scheme examines the geometry of the manifolds $R_n = \text{const}$ and $R_{-n} = \text{const}$ to determine the left and right states. It was seen in (104) and (105) that $\mathcal{M}_t^- < \mathcal{M}_t^+$ must hold if the (i, j)th cell can be used to compute the left state. It is possible for both states to be taken from one cell, depending on the local flow gradients. A possible choice for $\mathcal{M}_t$, which works well in practice, is

$$(130) \qquad\qquad \mathcal{M}_t \; = \; (\mathcal{M}_t^- + \mathcal{M}_t^+)/2 \; .$$

So far, the tacit assumption of smooth, shock-free flow has been made. The theory of RIM has been developed with the assumption that the flow gradients exist and are smooth. It is known that in gas-dynamical flows, discontinuities in the flow variables and their gradients may be present. The theory, nevertheless, can still be used for flows with such discontinuities. In the 1-D case, although the characteristics cannot propagate information across shocks, they can still be used on either side of shocks to determine the states that are related via the jump conditions. It is the generalization of the 1-D characteristic equations that leads to the concept of the Riemann problem. In the context of a Godunov scheme, discontinuities are assumed at every cell interface. In the smooth regions of the flow, these discontinuities are infinitesimally weak, and the characteristics are used to compute the numerical fluxes. To take care of the flow regions containing shocks, the characteristic problem is generalized to the Riemann problem. In effect, the characteristic equations are discretized to second-order accuracy where the flow is smooth and in a way which is consistent with the appropriate jump conditions when discontinuities are present.

In the multidimensional case the situation is similar. The RIM cannot propagate information through shocks or characteristic surfaces that contain derivative discontinuities. Nevertheless, they can be used on either side of these discontinuities to determine the states that are connected with the appropriate jump conditions. The easiest way of implementing this, although possibly not the most accurate, is to use

the left and right states, determined by the RIM, as the initial condition for a 1-D Riemann problem. Care must be taken so that the discretization of the equations is consistent via the jump conditions when shocks are present. This geometric picture also suggests the possibility of changing the unit vector **n** locally, so that it coincides with the unit normal of the discontinuity fronts. For example, consider a shock with unit normal **n**, locally. The RIM $R_{\pm n}$ = const on either side of the shock can be used to determine the states that are related with the jump conditions.

This procedure is reminiscent of the attempts to fit shocks in flows when the method of characteristics is used; see Moretti (1979). The analogy is not surprising, since the theory of RIM can be looked at as an extension of the method of characteristics to the general, multidimensional case.

It is also interesting to determine when the conventional MUSCL scheme, at least the version used here as a reference point, will give the same results as the multidimensional scheme. It is seen from (108), (114), (126), and (116) that the two schemes will coincide to *leading order*, if the left state can be taken from the left cell, the right state from the right cell, and in addition,

$$\text{(131)} \qquad \begin{aligned} \nu \cdot \nabla p - \rho a \nabla \cdot \mathbf{u} &= 0 , \\ a\nu \cdot \nabla \rho - \rho \nabla \cdot \mathbf{u} &= 0 , \end{aligned}$$

for both manifolds $R_{\pm n}$ = const. This cannot always be satisfied, but it now becomes clear why the conventional schemes give reasonable results in multidimensional flows. The terms in (131) can be taken to be very small and sometimes zero. This depends on the local flow conditions.

It should be noted here that the scheme based on the RIM decomposition is not meant to be the ultimate second-order multidimensional scheme that is better than all other schemes including the dimensionally split ones. The first author strongly believes that no such scheme exists. It turns out to be a very robust scheme without stability problems and it differs from most characteristic-based schemes in the special directions which are used to calculate the numerical fluxes. This difference may become important in some parts of the flow.

6. Numerical applications. The new multidimensional Godunov scheme developed in the previous section is used to compute two gas-dynamical flows on rectangular grids. The first case is the steady-state, regular shock reflection off a wall at low resolution. The second flow is a double Mach reflection of a planar-shock incident on an oblique surface. These two problems have been used extensively as test cases for a variety of numerical methods, and there are detailed comparisons of existing methods in the literature; e.g., see Woodward and Colella (1984) and Colella (1990). In all the calculations, a perfect gas is assumed, with constant, specific heat ratio equal to $\gamma = 1.4$.

The regular shock reflection has been used as a test case by many investigators. Colella (1990), among others, describes the initial and boundary conditions for this problem.

The computational domain is the rectangular domain $0 < x < 4$ and $0 < y < 1$. The lower boundary $y = 0$ is a reflecting wall, and at the right boundary $x = 4$, outflow conditions are imposed. The following inflow conditions are specified at the left boundary $x = 0$:

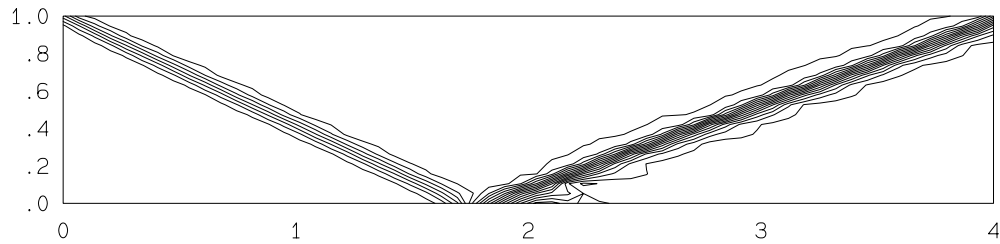$$\text{(132)} \qquad p = 1.0/1.4 , \quad \rho = 1.0 , \quad u = 2.9 , \quad v = 0 ,$$

FIG. 5. *Regular shock reflection. Pressure contour levels at time $t = 5$. There are 30 contour levels in the range $0.5 < p < 3.5$. The resolution is 60×20 cells.*

and at the top boundary $y = 1$, the following Dirichlet boundary condition is imposed:

$$(133) \qquad p = 1.52819 \,, \quad \rho = 1.69997 \,, \quad u = 2.61934 \,, \quad v = -0.50632 \,.$$

The initial condition in the entire domain is that of the inflow condition.

The computation is carried out with a CFL number of 0.40 until a steady state is achieved. Pressure contours at time $t = 5$ are shown in Figure 5. The pressure profiles have no overshoot and there are three cells within the shock. The present scheme employs no explicit, artificial dissipation as does the PPM scheme described by Colella and Woodward (1984), according to whom this additional dissipation is needed to suppress oscillations behind shocks that don't move with respect to the grid.

The double Mach reflection has been used by Woodward and Colella (1984) as a test problem for the comparison of existing numerical methods. The initial condition is that of a strong planar-shock incident on an oblique surface at a 30° angle. The shock Mach number is $M_s = 10$. The computational domain is the rectangular domain $0 < x < 4$ and $0 < y < 1$. The incident shock at time $t = 0$ is an oblique shock starting at the location $(x, y) = (1/6, 0)$ and forming a 60° angle with the positive x-axis. The lower boundary is a reflecting wall for $1/6 < x < 4$. At the small portion $0 < x < 1/6$ of the lower wall, a Dirichlet boundary condition is imposed, which corresponds to the initial post-shock flow. This artificial boundary condition ensures that the reflected shock is always attached to the point $(x, y) = (1/6, 0)$. The right boundary $x = 4$ is an outflow boundary, and the left boundary $x = 0$ is an inflow boundary whose inflow conditions are those of the initial post-shock flow. The conditions at the top boundary $y = 1$ are specified to be those corresponding to the motion of the initial planar shock wave.

Results of this unsteady calculation are shown at time $t = 0.20$. The solution is shown in Figures 6a and 6b, for a low-resolution computation corresponding to a 120×30 grid. In Figures 7a and 7b, the higher-resolution computation is shown. This corresponds to a 240×60 grid.

7. Conclusions. A new way of looking at multidimensional gas dynamics has been presented. The RIM wave decomposition, in general, provides more information and insight than the familiar characteristic decomposition. This decomposition is a local one and is not used to construct global solutions of the Euler equations, but it transforms the problem of integrating the Euler equations into a geometrical problem of integrating paths in spacetime. This is exactly what the method of characteristics achieves in 1-D flow and that is why the RIM decomposition can be considered as the extension of that method to the multidimensional case.
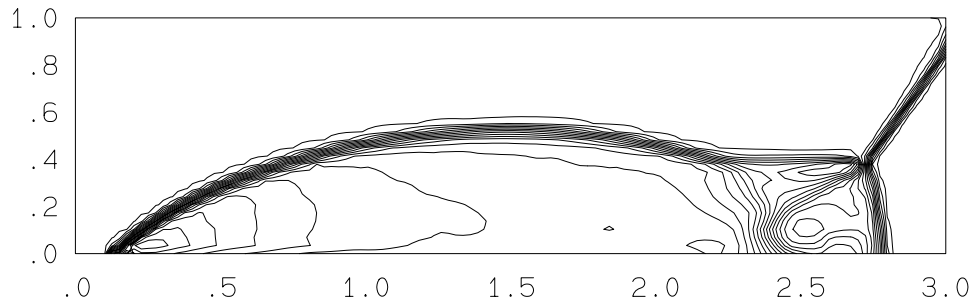
FIG. 6a. *Double Mach reflection. Density contour levels at time $t = 0.20$. There are 30 contour levels in the range $1.7 < \rho < 18.5$. The resolution is 120×30 cells.*
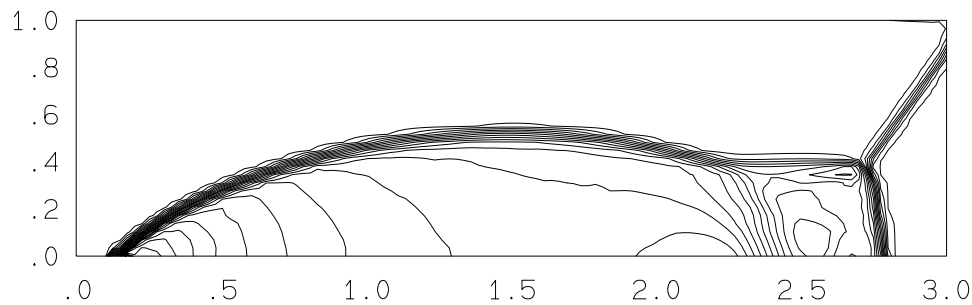

FIG. 6b. *Double Mach reflection. Pressure contour levels at time $t = 0.20$. There are 30 contour levels in the range $2 < \rho < 450$. The resolution is 120×30 cells.*
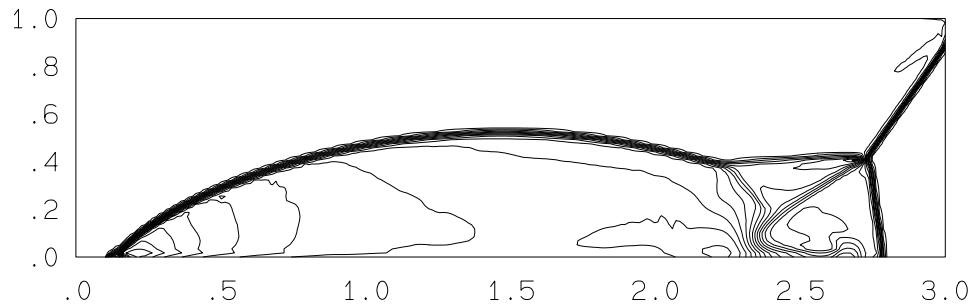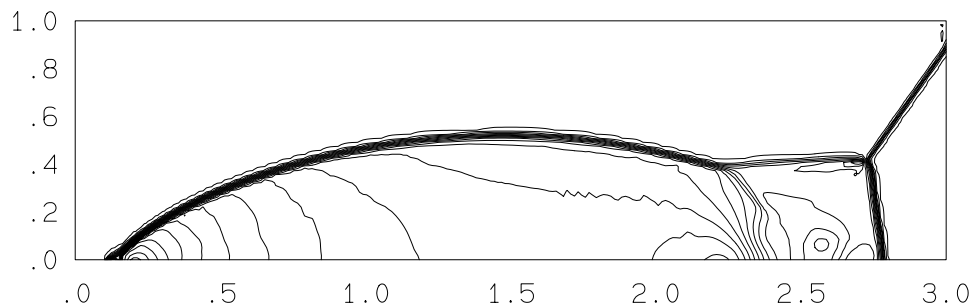

FIG. 7a. *Double Mach reflection. Density contour levels at time $t = 0.20$. There are 30 contour levels in the range $1.73 < u < 21.0$. The resolution is 240×60 cells.*

FIG. 7b. *Double Mach reflection. Pressure contour levels at time $t = 0.20$. There are 30 contour levels in the range $2 < u < 480$. The resolution is 240×60 cells.*

The theory allows the development of effective numerical schemes for multidimensional flows in a mathematically consistent way. There are many ways of implementing these ideas numerically. As an example, it was shown how a second-order MUSCL-type scheme can be modified to give a conservative, multidimensional, shock-capturing scheme for 2-D flows. The results from this scheme appear to be very close to those of conventional schemes, but a detailed study is needed.

REFERENCES

P. Colella and P.R. Woodward (1984), *The piecewise parabolic method (PPM) for gas dynamical simulations*, J. Comput. Phys., 54, pp. 174–201.

P. Colella (1990), *Multidimensional upwind methods for hyperbolic conservation laws*, J. Comput. Phys., 87, pp. 171–200.

R. Courant and D. Hilbert (1963), *Methods of Mathematical Physics, Vol.* II, Interscience, New York.

H. Deconinck, Ch. Hirsch, and J. Peuteman (1986), *Characteristic decomposition methods for the multidimensional Euler equations*, in Proceedings of the 10th International Conference on Numerical Methods in Fluid Dynamics, Beijing.

W.-S. Don and D. Gottlieb (1990), *Spectral simulations of an unsteady compressible flow past a circular cylinder*, Comput. Methods Appl. Mech. Engrg., 80, pp. 39–58.

K.O. Friedrichs and P.D. Lax (1965), *Boundary value problems for first order operators*, Comm. Pure Appl. Math., 18, pp. 355–388.

J. Glimm (1965), *Solutions in the large for nonlinear hyperbolic systems of equations*, Comm. Pure Appl. Math., 18, pp. 697–715.

S.K. Godunov (1959), *A finite difference method for the numerical computation of discontinuous solutions of the equations of fluid dynamics*, Mat. Sb., 47, pp. 271–306.

A. Harten (1983), *High resolution schemes for hyperbolic conservation laws*, J. Comput. Phys., 49, pp. 357–393.

A. Harten (1984), *On a class of high resolution total-variation-stable finite-difference schemes*, SIAM J. Numer. Anal., 21, pp. 1–23.

A. Harten, B. Engquist, S. Osher, and S.R. Chakravarthy (1987), *Uniformly high order accurate essentially non-oscillatory schemes*, III, J. Comput. Phys., 71, pp. 231–303.

Ch. Hirsch and C. Lacor (1989), *Upwind Algorithms Based on a Diagonalization of the Multidimensional Euler Equations*, AIAA Paper No. 89-1958, Buffalo, New York.

T. Kato (1975), *The Cauchy problem for quasi-linear symmetric hyperbolic systems*, Arch. Rational Mech. Anal., 58, pp. 181–205.

G. Moretti (1979), *The λ-scheme*, Comput. & Fluids, 7, pp. 191–205.

P.L. Roe (1981), *Approximate Riemann solvers, parameter vectors, and difference schemes*, J. Comput. Phys., 43, pp. 357–372.

P.L. Roe (1986), *Discrete models for the numerical analysis of time-dependent multidimensional gas dynamics*, J. Comput. Phys., 63, pp. 458–476.

J. Smoller (1983), *Shock Waves and Reaction-Diffusion Equations*, Springer-Verlag, New York.

G. Strang (1968), *On the construction and comparison of difference schemes*, SIAM J. Numer. Anal., 5, pp. 506–517.

B. van Leer (1979), *Towards the ultimate conservative difference scheme.* V. *A second-order sequel to Godunov's method*, J. Comput. Phys., 32, pp. 101–136.

B. van Leer (1984), *On the relation between the upwind-differencing schemes of Godunov, Engquist–Osher and Roe*, SIAM J. Sci. Stat. Comput., 5, pp. 1–20.

P.R. Woodward and P. Colella (1984), *The numerical simulation of two-dimensional fluid flow with strong shocks*, J. Comput. Phys., 54, pp. 115–173.